Cell Reports

Article

Super-resolution proximity labeling reveals anti-viral protein network and its structural changes against SARS-CoV-2 viral proteins

Graphical abstract

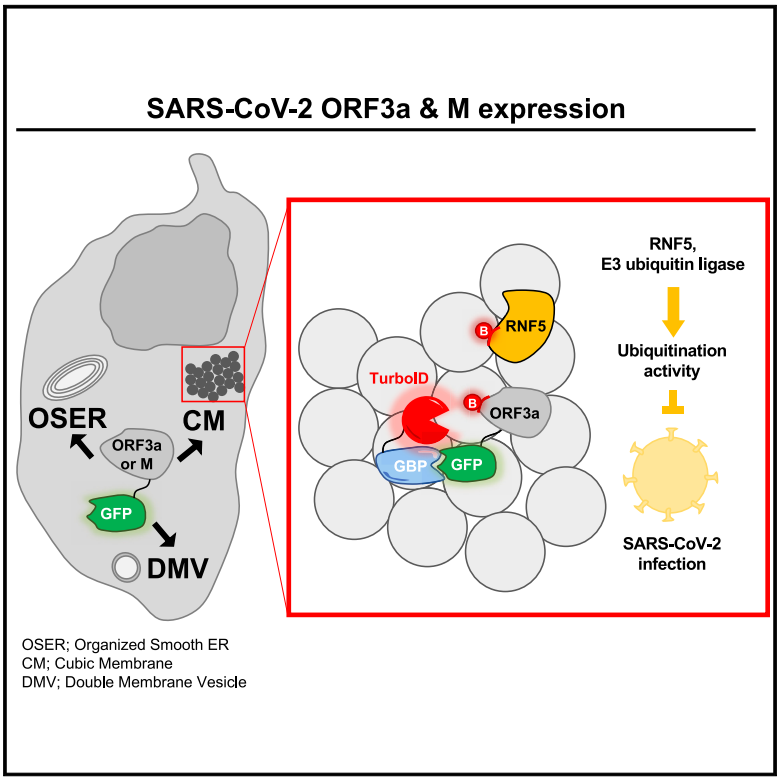

Authors

Yun-Bin Lee, Minkyo Jung, Jeesoo Kim, ..., Jong-Seo Kim, Ji Young Mun, Hyun-Woo Rhee

Correspondence

jongseokim@snu.ac.kr (J.-S.K.), jymun@kbri.re.kr (J.Y.M.), rheehw@snu.ac.kr (H.-W.R.)

In brief

Lee et al. introduce the super-resolution proximity labeling (*SR-PL*) method to identify the host interactome of viral proteins (ORF3a and M) in SARS-CoV-2. Through this approach, they discover that RNF5 plays a crucial role by ubiquitinating ORF3a, leading to a decrease in the infection rate of SARS-CoV-2.

Highlights

- ORF3a and M of SARS-CoV-2 perturb ER structure
- ORF3a and M interactomes are identified through *SR-PL*
- RNF5 ubiquitinates ORF3a
- RNF5 expression lowers SARS-CoV-2 infection rate

Lee et al., 2023, Cell Reports *42*, 112835
August 29, 2023
https://doi.org/10.1016/j.celrep.2023.112835

CellPress

Cell Reports

CellPress
OPEN ACCESS

Article

Super-resolution proximity labeling reveals anti-viral protein network and its structural changes against SARS-CoV-2 viral proteins

Yun-Bin Lee,[1] Minkyo Jung,[2] Jeesoo Kim,[3,4] Afandi Charles,[5] Wanda Christ,[6] Jiwoong Kang,[1] Myeong-Gyun Kang,[1] Chulhwan Kwak,[1] Jonas Klingström,[6,7] Anna Smed-Sörensen,[5] Jong-Seo Kim,[3,4,*] Ji Young Mun,[2,*] and Hyun-Woo Rhee[1,3,8,*]

[1]Department of Chemistry, Seoul National University, Seoul 08826, Republic of Korea
[2]Neural Circuit Research Group, Korea Brain Research Institute, Daegu 41062, Republic of Korea
[3]School of Biological Sciences, Seoul National University, Seoul 08826, Republic of Korea
[4]Center for RNA Research, Institute for Basic Science, Seoul 08826, Republic of Korea
[5]Division of Immunology and Allergy, Department of Medicine Solna, Karolinska Institutet, Karolinska University Hospital, 17164 Stockholm, Sweden
[6]Centre for Infectious Medicine, Department of Medicine Huddinge, Karolinska Institutet, 14183 Stockholm, Sweden
[7]Division of Molecular Medicine and Virology, Department of Biomedical and Clinical Sciences, Linköping University, 581 83 Linköping, Sweden
[8]Lead contact
*Correspondence: jongseokim@snu.ac.kr (J.-S.K.), jymun@kbri.re.kr (J.Y.M.), rheehw@snu.ac.kr (H.-W.R.)
https://doi.org/10.1016/j.celrep.2023.112835

SUMMARY

Severe acute respiratory syndrome coronavirus 2 (SARS-CoV-2) replicates in human cells by interacting with host factors following infection. To understand the virus and host interactome proximity, we introduce a super-resolution proximity labeling (*SR-PL*) method with a "plug-and-playable" *PL* enzyme, TurboID-GBP (GFP-binding nanobody protein), and we apply it for interactome mapping of SARS-CoV-2 ORF3a and membrane protein (M), which generates highly perturbed endoplasmic reticulum (ER) structures. Through *SR-PL* analysis of the biotinylated interactome, 224 and 272 peptides are robustly identified as ORF3a and M interactomes, respectively. Within the ORF3a interactome, RNF5 co-localizes with ORF3a and generates ubiquitin modifications of ORF3a that can be involved in protein degradation. We also observe that the SARS-CoV-2 infection rate is efficiently reduced by the overexpression of RNF5 in host cells. The interactome data obtained using the *SR-PL* method are presented at https://sarscov2.spatiomics.org. We hope that our method will contribute to revealing virus-host interactions of other viruses in an efficient manner.

INTRODUCTION

In the current coronavirus disease 2019 (COVID-19) pandemic, caused by severe acute respiratory syndrome coronavirus 2 (SARS-CoV-2), it is essential to understand the host protein network for the viral proteins of SARS-CoV-2 to prevent or treat COVID-19. The viral genome of SARS-CoV-2 encodes 29 proteins: 16 nonstructural proteins (NSP1–16), 4 structural proteins (spike protein [S], membrane protein [M], envelope protein [E], and nucleocapsid protein [N]), and 9 accessory proteins (open reading frame 3a [ORF3a], ORF3b, ORF6, ORF7a, ORF7b, ORF8, ORF9b, ORF9c, and ORF10). NSPs participate in the formation of the replicase-transcriptase complex,[1] and structural proteins (S, M, E, and N) form a viral particle unit that can mediate the transfer of viral RNA across cells.[1] The 9 accessory proteins (ORFs) are translated from the viral RNA and mediate the assembly of viral components in infected cells. Many ORFs target the endomembrane system; however, their local molecular functions and interaction networks are not clearly understood. Currently, a handful of studies have shown that ORFs can turn off the host innate immune system during viral replication by hijacking autophagosome processes[2] or by acting as an interferon antagonist.[3] Notably, components of the host immune system, such as the NOD-like receptor protein 3 (NLRP3) inflammasome, can be activated by ORF3a expression[4]; however, it is not clearly understood which host factors can recognize these viral proteins. Since mutations in ORFs can considerably affect viral replication efficiency in host cells,[5] a clear elucidation of the interactome of these proteins could lead to the development of anti-viral or anti-inflammation therapeutics to overcome the pandemic.

To identify viral protein-host protein interactions, affinity-purification mass spectrometry (AP-MS) analysis was conducted for SARS-CoV-2.[1,6] AP-MS results showed interaction partners with strong binding affinity to the viral proteins of interest (vPOIs); however, these interactome data may also include artificial protein-protein interactions that do not occur in live cells because these experiments were conducted using cell lysates isolated in artificial lysis buffer conditions. To overcome these limitations,

proximity labeling (PL) methods are based on an enzymatic biotinylation reaction using *in-situ*-generated reactive biotin species by genetically expressed enzymes. Examples of these enzymes include engineered ascorbate peroxidase (APEX),[7] promiscuous biotin ligase (BioID),[8] and TurboID, an engineered biotin ligase with faster kinetics.[9] Because the biotinylation reaction induced by PL enzymes occurs in living cells and the labeling radius of the reactive biotin species (biotin-phenoxy radical and biotin-AMP) is less than 50 nm, MS analyses of endogenous proteins biotinylated by PL enzymes can accurately reflect the physiological interactome of the POI that is genetically expressed alongside these enzymes.

PL has been used to identify the host interactome of viral proteins, including coronaviruses[10] and SARS-CoV-2.[11–15] Although this method identifies various important host proteins that support the viral life cycle, results from the conventional PL workflow may contain false positive findings. Currently, most current works including viral interactome studies using PL utilize conventional mass analysis, which detects the "non-biotinylated peptides" of streptavidin bead-enriched proteins that usually provide ambiguous and low-resolution results. This conventional PL method can misidentify artificially interacting proteins in the lysis buffer as biotinylated proteins (false positives). To overcome the limitations of conventional PL methods, scientists have developed a method for the mass detection of "biotinylated" PTM sites for APEX (e.g., Y+331 Da) and BioID/TurboID (e.g., K+226 Da), which reflect true biotinylation events at the single-amino acid residue level.[16–18] Since this method can provide clear biotinylation modification information at the single amino acid residue level, we refer to this method as super-resolution PL (*SR-PL*), which is analogous to the super-resolution imaging method that can detect single-molecule fluorescence, while conventional imaging methods provide blurred results. Notably, both conventional and *SR* methods for imaging and PL utilize the same molecules (e.g., fluorophores or biotin probes), but the analysis workflow is different (Figure 1A). We have previously applied *SR-PL* to reveal the local proteome of interest, such as that in the inner mitochondrial membrane,[18] the mitochondria-endoplasmic reticulum (ER) contact site,[19] and the liver-specific secretome.[20] We also applied this technique to identify novel rapamycin-interacting partners,[16] NSUN2 in the mitochondrial matrix[21] and EXD2 in the outer mitochondrial membrane.[22]

Herein, we show that *SR-PL* is an efficient method for revealing the virus-host interactome of SARS-CoV-2. We also confirmed that the "plug-and-play" GFP and GFP-binding nanobody protein (GBP) system, which was previously utilized for efficient electron microscopy (EM) imaging of POI-GFP with APEX2 in zebrafish.[23] It is noteworthy that GFP-POI and GBP-TurboID have been successfully applied to identify the interactome of POIs in live models, such as zebrafish[24] and *C. elegans*.[25] This system can be utilized for the efficient mapping of the host protein network of viral proteins with *SR-PL*. Using this devised tool, we successfully revealed the host interactome of the accessory protein (ORF3a) and structural protein (M) of SARS-CoV-2. Among the host factors of these proteins, we confirmed that RNF5, an E3 ubiquitin ligase, decreased the infectivity of live SARS-CoV-2 in human cells *in vitro*. We investigated the RNF5 interactome with *SR-PL* to understand its function at the molecular level. We found that unique biotin-labeled sites of *SR-PL* can not only reveal the proximal interactome but also suggest possible structural changes. Overall, we believe that our *SR-PL* analysis provides meaningful and unique insights into the viral protein interactome.

RESULTS

GFP-tagged SARS-CoV-2 structural and accessory proteins target specific organelles

To confirm the subcellular localization of the SARS-CoV-2 proteins, we prepared 14 constructs of vPOIs tagged with GFP using a 13-amino acid linker (GAPGSAGSAAGSG) (Figures 1B and S1A). These GFP-tagged constructs were applied to *SR-PL* using a GFP/GBP system (Figure 1B). Confocal imaging showed that the GFP-tagged vPOIs were well expressed. Unlike NSPs, structural and accessory proteins target specific organelles. NSP7, NSP8, and NSP9 showed whole-cell expression patterns (Figure S1B), indicating that these proteins were diffused throughout the cell and did not specifically interact with certain organelles, possibly because of the lack of viral RNAs. In contrast, M, N, ORF3a, ORF3b, ORF6, ORF7b, ORF9b, and ORF9c showed organelle-specific localization patterns (Figure 1C), indicating that these proteins interact with the host proteins of specific organelles. Among these constructs, we observed that the expression patterns of ORF3a and M merged with those of both an ER marker protein, SEC61B (Figure S1C), and an ER endogenous protein, calnexin (Figure S1D), which supports their basal localization in the ER.

In addition, we confirmed that GFP-tagged vPOIs (i.e., ORF3a, ORF6, ORF7b, and M) merged with FLAG-tagged vPOIs in co-expressing cells, indicating that both vPOIs were targeted to the ER by increasing perturbation of its structure (Figure S1E). Additionally, we confirmed that GFP-tagged vPOIs (i.e., ORF3a and M) were well expressed in A549 cells (Figure S1F), and the pattern of vPOI expression was similar to that in HEK293-AD cells (Figure 1C). Consistent with a previous study showing that the N is associated with stress granules,[1] confocal imaging co-expressing N and G3BP1 (stress granule marker protein)[26,27] showed that the two patterns were clearly merged, representing a stress granule pattern (Figure S1G). These experiments confirmed that the established GFP-tagged structural and accessory protein constructs were suitable for further interactome studies.

The GFP/GBP system can be used to identify the SARS-CoV-2 interactome in live cells. We utilized the GFP and GBP "plug-and-play" system[23–25] for the interactome analysis of vPOI-GFP by co-expression of TurboID-GBP via *SR-PL* workflow (Figures 1A and 1B). To confirm the specific binding between vPOI-GFP and TurboID-GBP, M, N, ORF3a, ORF6, and ORF7b were selected. The confocal image patterns of cells co-expressing vPOI-GFP and TurboID-GBP were identical to those of cells expressing vPOI-GFP alone (Figures 1C, 1D, and S2A), demonstrating that GFP and GBP bound well and that the patterns of the biotinylated proteins merged with the GFP and GBP patterns. Thus, we confirmed that the co-expressed TurboID-GBP had a strong and specific binding interaction

CellPress
OPEN ACCESS

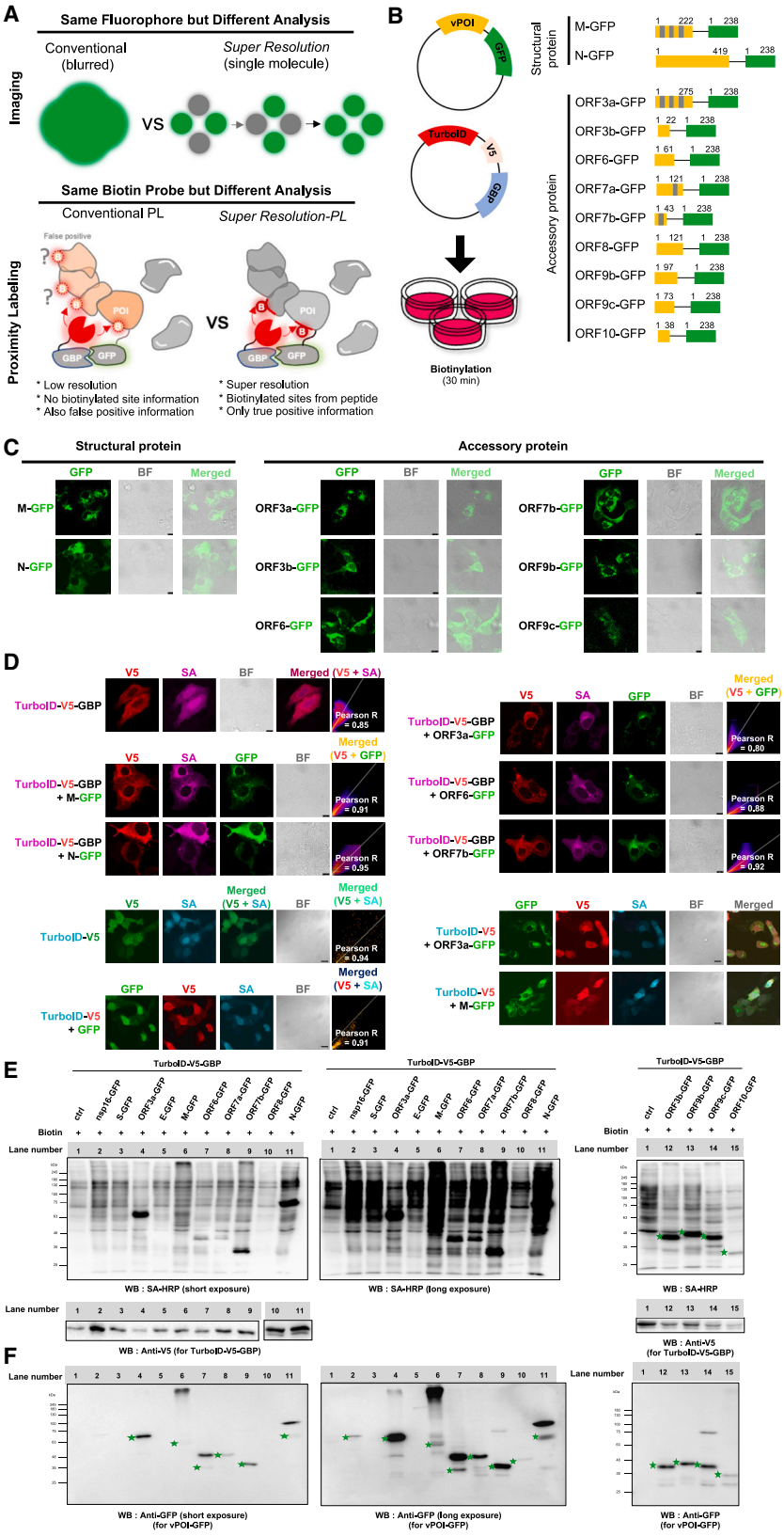

Figure 1. *In situ* biotinylation of "plug-and-play" TurboID-GBP with vPOI-GFP of SARS-CoV-2

(A) Comparison between *super-resolution* imaging and *super-resolution* proximity labeling (*SR-PL*).

(B) *In situ* biotinylation of TurboID-V5-GBP with viral protein of interest (vPOI)-GFP. Predicted TM domains by TMHMM program are shown in light gray.

(C) Confocal microscopy images of vPOI-GFP constructs in HEK293-AD cells. vPOIs are M, N, ORF3a, ORF3b, ORF6, ORF7b, ORF9b, and ORF9c. Scale bars: 10 μm. BF, bright field.

(D) Confocal microscopy images of vPOI-GFP and TurboID-V5-GBP (or TurboID-V5) in HEK293-AD cells. Scale bars: 10 μm. BF, bright field. Additional images are shown in Figure S2A.

(E) Streptavidin-horseradish peroxidase (SA-HRP) and anti-V5 western blotting results under the co-expression of vPOI-GFP and TurboID-V5-GBP in HEK293T cells.

(F) Anti-GFP western blotting results of the same samples as (E). Bands of the expected molecular weight of each vPOI-GFP construct are marked with green asterisks. Raw images of blot results are shown in Figures S2B–S2D.

(C–F) Representative data from one of three experiments.

with vPOI-GFP and did not appear to interrupt the targeting of vPOI-GFP to specific organelles.

Western blot analysis of proteins biotinylated by TurboID-GBP and detected using streptavidin-horseradish peroxidase (SA-HRP) revealed that the biotinylated protein patterns of TurboID-GBP were altered when co-expressed with GFP-tagged M, N, ORF3a, ORF3b, ORF6, ORF7a, ORF7b, ORF9b, ORF9c, or ORF10 (Figures 1E, 1F, and S2B–S2D). The change in SA-HRP western blot patterns of the proteins biotinylated by the *PL* enzyme[16] may indicate that the neighboring proteins around TurboID-GBP were significantly altered when TurboID-GBP was translocated to co-expressed vPOI-GFP in the same cell. These experiments also showed that the GFP-tagged structural and accessory proteins of SARS-CoV-2 may be surrounded by different host proteins in cells and that these proteins may be readily biotinylated by TurboID and identified using MS via the *SR-PL* workflow (Figure 1A).

ORF3a and M proteins of SARS-CoV-2 destructively perturb the ER membrane organization

Among the structural and accessory proteins that exhibited an ER-targeting pattern (Figures S1C and S1D), ORF3a and M contained three transmembrane (TM) domains (Figures 1B and S3A), and both proteins showed a similar alteration of protein band patterns in western blot analysis, with a larger molecular weight than expected (Figure 1F). ORF3a$^{SARS\text{-}CoV\text{-}2}$ shows 85.1% sequence similarity with ORF3a$^{SARS\text{-}CoV\text{-}1}$, which exhibits ion transport activity and induces NLRP3 inflammasome activation.[4] ORF3a$^{SARS\text{-}CoV\text{-}2}$ also possesses pro-apoptotic activity.[28] Similarly, the M$^{SARS\text{-}CoV\text{-}2}$ shows 96.4% sequence similarity with the M$^{SARS\text{-}CoV\text{-}1}$, which has been reported to target the ER, the ER-Golgi intermediate compartment, and the Golgi apparatus and is associated with apoptosis[29] and nuclear factor-κB (NF-κB) signaling.[30] We hypothesized that these proteins might perturb the ultrastructure of the endomembrane system, as many viral proteins have been shown to target the endomembrane systems of host cells.[31]

To test this hypothesis, we conducted correlative light and EM (CLEM) experiments using ORF3a-GFP- and M-GFP-transfected cells (Figure 2A). Similar to ORF3a$^{SARS\text{-}CoV}$-expressing cells[32] and the SARS-CoV-infected cells,[33] ORF3a and M proteins largely disrupted the ER. In CLEM imaging of ORF3a-GFP, increased cubic membrane (CM, also denoted as convoluted membrane) structure formation was observed (Figure 2B). In CLEM imaging of M-GFP (Figure 2C), we observed severe formation of multilamellar bodies (MLBs) at the ER membrane and electron-dense autophagic vesicles (black arrows in Figure 2C). In addition, we conducted CLEM imaging of ORF3a and M co-expressing cells, which also showed disrupted ER patterns, including CM and double-membrane vesicle (DMV) structures (Figure S3B). Additionally, while only the expression of GFP or mCherry did not largely disrupt the ER pattern, and normal levels of MLBs were only detected (Figures S3C and S3D), untagged ORF3a or M expression disrupted the ER structure by the formation of DMVs (Figures S3E and S3F). To confirm that the endomembrane system was perturbed by ORF3a and M, we prepared an APEX-mediated diaminobenzidine (DAB)-stained sample[34] using SEC61B-APEX2, which showed that the ER structure was largely damaged when ORF3a-GFP was expressed (Figure S3G).

Additionally, we prepared ORF3a and M constructs with APEX2 directly tagged to the C terminus of the vPOIs (Figures 2D and 2E) and used them for the EM imaging of transfected cells following APEX-mediated DAB staining.[34] DAB staining of ORF3a-APEX2 clearly showed CM structure formation (Figures 2F and S3H). Notably, CM structures are also formed in coronavirus-infected cells[35,36] and are considered neo-organelles for the assembly of viral proteins.[37] Additionally, in ORF3a-APEX2-expressing cells, the DMV (red arrows in Figure 2F) was detected by APEX2-DAB staining near the ER and mitochondria, which was also observed in untagged ORF3a-expressing cells (Figure S3E). Because DMV formation is believed to house the replication complexes of various RNA viruses,[38–40] our results imply that ORF3a plays an important role in the formation of ER-derived compartments (i.e., CM and DMV) that can be related to viral replication in host cells.

Similarly, the ER was clearly disrupted in M-APEX2-expressing cells (Figures 2G and S3I) and appeared to curl into whorl patterns, also termed organized smooth ER (OSER), which was also reproducibly observed in untagged, M-expressing cells (Figure S3F). These OSER patterns have also been observed in SARS-CoV-infected cells,[33] herpes simplex virus-infected cells,[41] and ER stress-induced cells.[42,43] In our study, these structures were not detected in untransfected cells (Figures S3I and S3J). Moreover, we confirmed that the structures of the ER, Golgi, and mitochondria did not change in SEC61B-APEX2- or APEX2-expressing cells (Figure S3J). Therefore, our EM results imply that ORF3a and M may largely contribute to the generation of ER-derived compartments[44–46] for efficient viral assembly and replication by remodeling the ER systems. To identify the host proteins involved in this process, we conducted an *in cellulo* interactome analysis of ORF3a-GFP and M-GFP with TurboID-GBP via the *SR-PL* workflow.

ORF3a and M interactomes showed perturbed proteomic landscape at the ER membrane

For the mass spectrometric analysis, we used the aforementioned *SR-PL* method to obtain an accurate interactome map of the ORF3a and M proteins. To obtain the biotinylated peptidome, HEK293T cells co-expressing vPOI-GFP and TurboID-GBP and control HEK293T cells (Figure 3A) were treated with biotin (50 μM, 30 min). As control samples, we prepared HEK293T cells co-expressing vPOI-GFP and TurboID, which have no physical interaction between the co-expressed proteins, and all the biotinylated peptides in these control samples can be regarded as background-labeled proteins of TurboID, which are abundantly expressed in the cytosol under ER perturbation conditions by expression of vPOI-GFP. We also prepared unconjugated GFP + TurboID-GBP co-expressing cells, which could provide a possible interactome for GFP and GBP in the cytosol.

We obtained 3,796 and 3,498 peptides biotinylated at the lysine residue (K+226) from triplicate ORF3a (ORF3a-GFP + TurboID-GBP) and M (M-GFP + TurboID-GBP) samples, respectively. We also obtained 2,865, 3,889, and 4,969

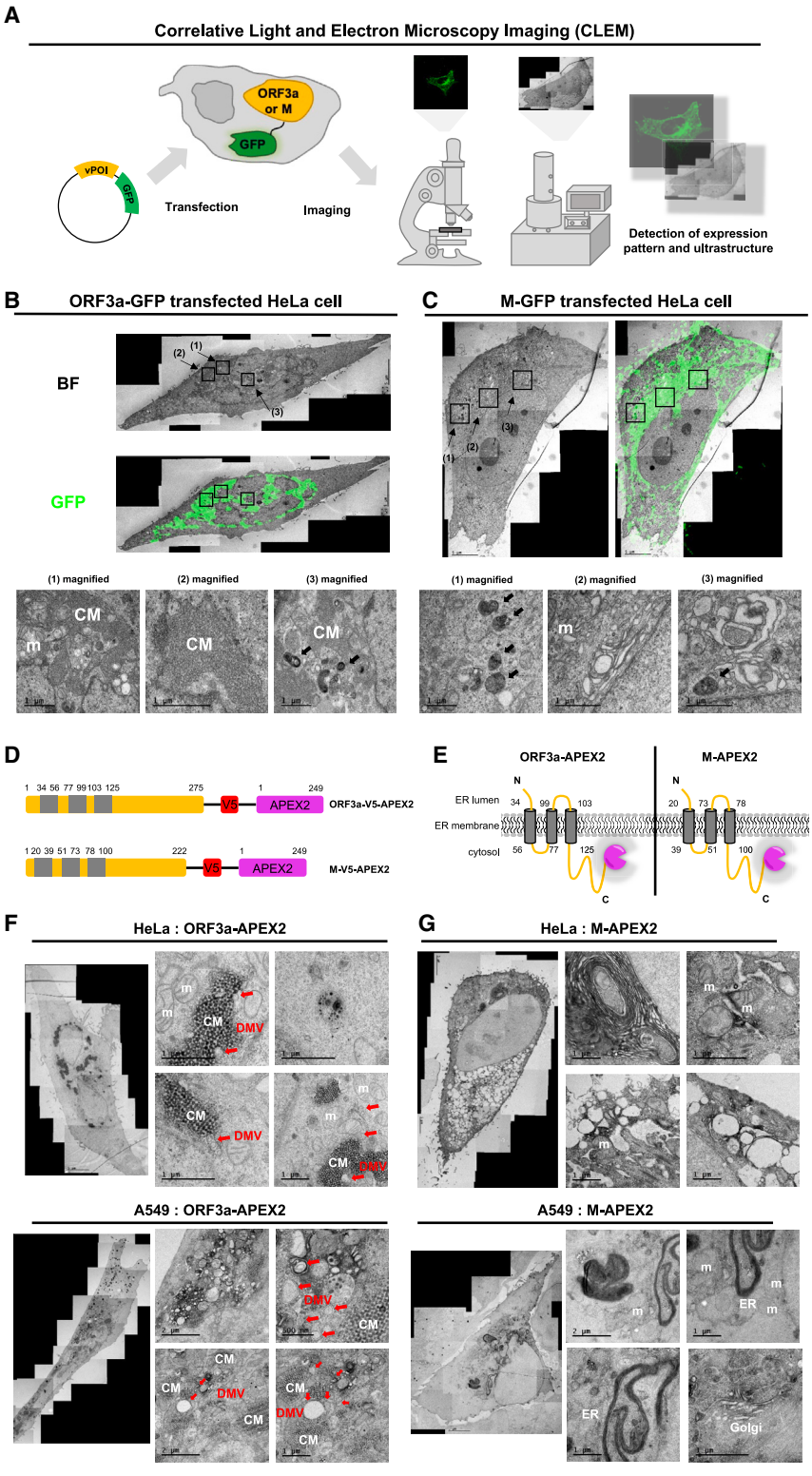

Figure 2. EM results of ORF3a and M protein of SARS-CoV-2-expressing cells

(A) Schematic view of CLEM experiments.

(B) CLEM images of ORF3a-GFP-transfected HeLa cells. Scale bars: 1 μm. Electron-dense autophagic vesicles are marked with black arrows (B and C). Distinct membrane structures were observed with higher magnification, and magnified areas are marked with box numbers (B and C).

(C) CLEM images of M-GFP-transfected HeLa cells. Scale bars: 1 μm.

(D) Schematic view of ORF3a-APEX2 and M-APEX2. TM domains are shown in light gray.

(E) Proposed membrane topology of ORF3a-APEX2 and M-APEX2 at the ER membrane.

(F) EM images of ORF3a-APEX2-transfected HeLa cells and A549 cells. Scale bars: 500 nm–2 μm. Additional EM images are shown in Figure S3H.

(G) EM images of M-APEX2-transfected HeLa cells and A549 cells. Scale bars: 1–2 μm. Additional EM images are shown in Figure S3I.

(B, C, F, and G) Cubic membrane, double-membrane vesicle structures, and mitochondria are indicated as "CM," red arrows, and "m," respectively. Representative data from one of two experiments.

biotinylated peptides from control samples (ORF3a-GFP + TurboID; M-GFP + TurboID; GFP (control) + TurboID-GBP-expressing cells), respectively. The replicate samples showed high similarity and clustered with each other, confirming the reproducibility of the experiment (Figures S4A–S4F). From the comparative analysis of the ORF3a and M samples with the control samples, 470 and 520 peptides were selected as ORF3a- and M-specific biotinylated peptides, respectively. (Figures 3B and 3C; Data S1 and S2). Among these, we selected 224 (185 proteins) and 272 peptides (226 proteins) that were exclusively identified in ORF3a and M samples, respectively. These exclusively biotin-labeled peptides were reproducibly observed in all triplicate samples of ORF3a:TurboID or M:TurboID, and none of these labeled peptides were observed in the control samples (Figure S4G). The selection of the ORF3a and M interactome is summarized in a flowchart (Figure 3B).

The MS signal intensities of peptides 224 and 272 are shown as yellow dots in the volcano plots (Figure 3D; Data S1 and S2). In particular, the top 20 biotinylated sites based on MS signal intensity are shown as dots in the volcano plots (Figure 3D). The major population of interactomes for ORF3a and M comprise endomembrane system proteins, suggesting that ORF3a and M are primarily localized in the ER. Because exclusive proximity biotinylation can occur only in very close proximity, these exclusively biotinylated proteins should be very closely situated to ORF3a and M proteins. Each exclusively

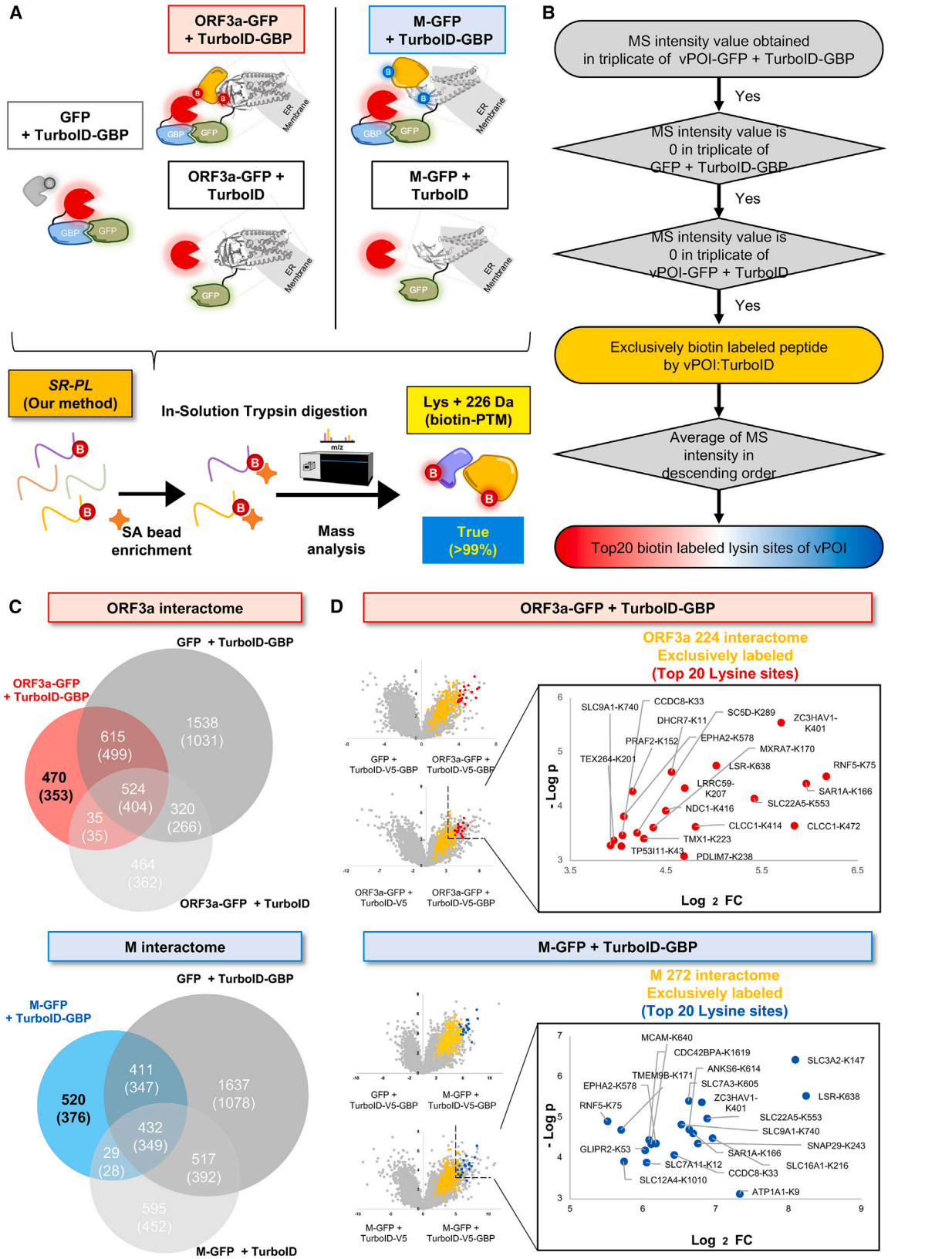

(legend on next page)

biotin-labeled peptide was sorted as shown in the Venn diagram and volcano plots. These proteins (e.g., CLCC1 and SLC22A5) have already been characterized as interaction partners of ORF3a and/or M (detailed information is provided in Data S1). Notably, CLCC1 (four sites exclusively labeled by ORF3a:TurboID) and SLC12A2 (three sites exclusively labeled by M:TurboID) showed multiple exclusively biotin-labeled sites, strongly indicating that the ORF3a and M proteins interact with the corresponding ER membrane proteins.

SR-PL reveals topology of TM proteins interacting with ORF3a and M

Among the 185 filtered proteins for the ORF3a interactome, 23.2% were located in the plasma membrane, and 60% were located in the endomembrane (Figures 4A and S4H). Among the 226 filtered proteins of the M interactome, 44.2% were located in the plasma membrane, and 40.3% were located in the endomembrane (Figures 4A and S4H). According to Gene Ontology analysis, proteins associated with SNARE interactions in vesicular transport were highly enriched among the 185 proteins of the ORF3a interactome and the 226 proteins of the M interactome (Figures 4B and S4I). From these analyses, we can see that the molecular functions of ORF3a and M are highly related to the localization and transport of other substances within the endomembrane of host cells.

To further our understanding of these interactions, we filtered the top 20 most strongly biotinylated peptides (red or blue dots in Figure 3D) among the ORF3a and M interactomes. Twenty filtered peptides of the ORF3a interactome were classified according to their localization and function (Figure 4C). Surprisingly, 12 of these 20 peptides (60%) overlapped with the recently identified mitochondrial-associated membrane (MAM) proteome as determined using Contact-ID.[19] This suggests that ORF3a is localized in the MAM, which is consistent with a previous host interactome analysis of SARS-CoV-2 using the co-immunoprecipitation (coIP) method.[47] MAM-enriched ORF3a interactome proteins were associated with vesicle transport (BET1, USE1, and SAR1A), lipid synthesis, and steroid binding and processes (DHCR7 and SCD5). We postulated that ORF3a might be involved in the regulation of vesicle trafficking at the MAM to support viral assembly and egress processes, similar to other viral proteins that target the MAM, such as the NS5A and NS5B proteins in the hepatitis C virus.[48] Moreover, several ion transport proteins that are part of the endomembrane system (CLCC1, SLC16A1, and SLC22A5) were identified in the ORF3a interactome. Based on previous findings that ORF3a of SARS-CoV regulates ion channels at the ER membrane[49,50] and that ORF3a of SARS-CoV-2 is related to Ca^{2+} and K^{+} channels[51] but does not form ion channels,[52] we postulated that ORF3a may closely localize at the subdomain of the ER where ion transport protein clusters.

Similarly, the top 20 filtered peptides of the M interactome were classified based on their localization and molecular functions (Figure 4D). Among these, those associated with ion transport (i.e., ATP1A1, SLC3A2, and SLC7A3) were highly enriched in the M interactome. Several proteins related to membrane integrity (i.e., CCDC8, CDC42BPA, and EPHA2) were highly enriched in the M interactome. Proteins that form SNARE complexes (i.e., BET1, VAMP7, and STX4) have been identified as the M interactome. This may influence ER vacuolization and apoptosis associated with M proteins.[29]

The identification of membrane protein topologies is crucial for understanding their domain-wise functions on either side of the membrane. In our study, the topological information of the biotin-labeled membrane proteins was easily extracted. Using our *SR-PL* method, we obtained MS data that included the biotinylation sites of each digested peptide. All digested peptides isolated following SA bead enrichment had at least one biotin-modified site on the lysine (K) residue. Since TurboID-GBP biotinylation occurs via the cytosolic regions of the protein, biotinylated sites on the proximal interacting proteins of vPOI-GFP logically face the cytosol. We then obtained membrane topological information for proteins harboring a TM domain using MS data. Using similar approaches, we have successfully revealed the topologies of the inner mitochondrial membrane[16] and MAM proteins.[19] Using this workflow (Figure 4E), 15 and 13 TM proteins were identified in the ORF3a and M interactomes, respectively; the biotinylation sites and topology of these proteins are shown in the figures (Figures 4F, S4J, and S4K). For example, K152 of PRAF2 and K223 of TMX1 matched well with previously characterized topologies. Based on these results, confirming the reliability of the *SR-PL* data, we propose hitherto unknown topologies of multiple ORF3a- or M-interacting membrane proteins (yellow proteins in Figure 4F).

Ubiquitination activity of RNF5 could suppress SARS-CoV-2 infection

In the ORF3a interactome, RNF5 exclusively showed biotin-labeled sites (K75) by ORF3a:TurboID, which was also shown in the M interactome (Figure 3D). This finding is interesting because RNF5 is an ER-anchored E3 ubiquitin protein ligase involved in the regulation of autophagy during bacterial infections.[53] Interestingly, RNF5 is involved in the inflammatory response[54] and regulates the anti-viral response of the outer mitochondrial protein MAVS,[55–58] which implies that RNF5 may

Figure 3. Mass analysis of host interactome of ORF3a and M protein of SARS-CoV-2 by *SR-PL*

(A) Schematic view of five groups of samples for mass analysis: TurboID-GBP + GFP, TurboID-GBP + ORF3a-GFP, TurboID + ORF3a-GFP, TurboID-GBP + M-GFP, and TurboID + M-GFP.

(B) Flowchart showing the classification process of exclusively biotin-labeled ORF3a and M interactome.

(C) Venn diagram of the *SR-PL*-detected biotinylated peptides of ORF3a, M, and control samples. The number of proteins is presented in parentheses below. See detailed information in Figure S4G.

(D) Enrichment of the *SR-PL*-detected biotinylated peptides by TurboID-GBP in the samples of ORF3a-GFP or M-GFP. x axis: log2 value of fold change of mass signal intensities; y axis: −log10 value of p value. Gene names of the top 20 biotinylated Lys sites of ORF3a or M sample are shown in the volcano plot. See detailed information in Data S1 and S2.

A

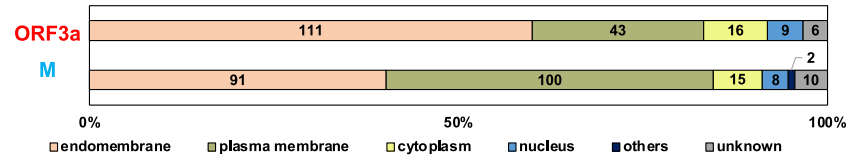

B

ORF3a interactome GO analysis	Examples of Protein	Enrichment FDR
Steroid biosynthesis	CYP51A1, NSDHL	7.6E-05
SNARE interactions in vesicular transport	SNAP29, BET1	5.4E-04
Notch signaling pathway	NOTCH2, ADAM17	6.4E-03
Choline metabolism in cancer	PIP5K1C, PTDSS1	4.0E-02
Endocytosis	CAV1, RAB7A	8.7E-03

M interactome GO analysis	Examples of Protein	Enrichment FDR
SNARE interactions in vesicular transport	BET1, VAMP7	3.8E-06
Steroid biosynthesis	SOAT1, NSDHL	1.9E-03
Adherence junction	PVRL3, SRC	2.5E-02
Hormone signaling pathway	NOTCH2, SRC	3.4E-02
Endocytosis	RAB11A, ARF6	5.2E-04

C

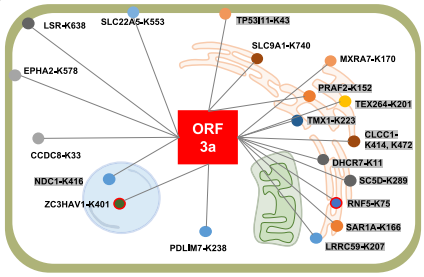

D

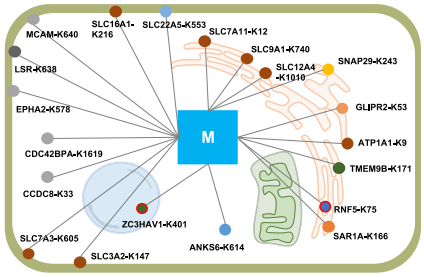

Protein transport and chaperone
Vesicle transport
Membrane integrity
Others
Autophagy/quality control
Protein degradation
Antiviral/immune signaling
Unknown
Redox reaction
Ion transport
Lipid synthesis and steroid binding/process
Proteins characterized as interacting with viral proteins

E

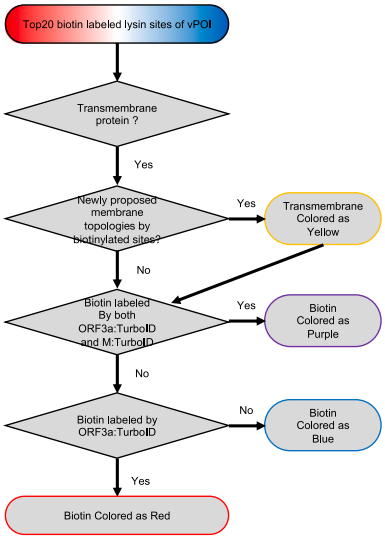

F

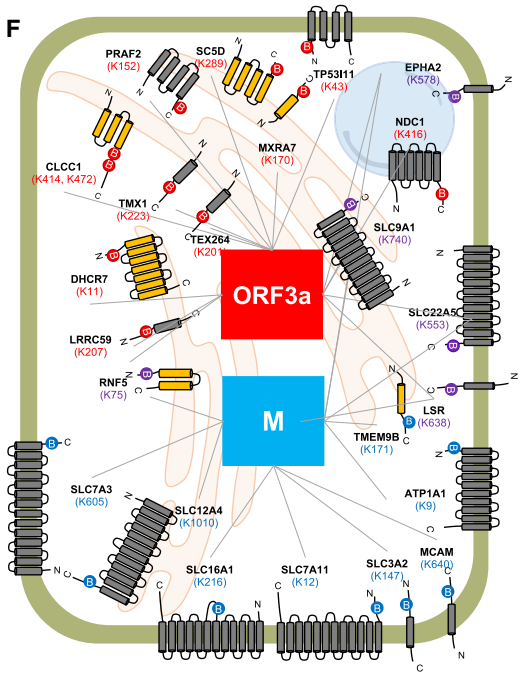

(legend on next page)

orchestrate the innate defense response against infections. Because the molecular function of RNF5 in SARS-CoV-2 has not yet been fully characterized, we conducted further studies to reveal its functional relationship with SARS-CoV-2 proteins. Confocal microscopy experiments using cells showed that RNF5 was embedded in the ER and spread throughout the whole ER compartment (Figure S5A). However, the pattern of RNF5 was largely altered by ORF3a and M expression and co-localized with the respective viral proteins (Figures 5A, S5B, and S5C). Co-localization of ORF3a and RNF5 was identified in the split-GFP system (Figures 5B and S5D). This implies that RNF5 may be activated when the ER is destroyed by ORF3a and M protein expression.

Because RNF5 has been characterized as an E3 ubiquitin ligase with anti-viral effects, we hypothesized that RNF5 could ubiquitinate ORF3a during SARS-CoV-2 infection. Treatment with a proteasome inhibitor (MG132) increased the expression of ORF3a and M (Figures S5E and S5F). Western blot analysis after coIP showed that overexpression of RNF5 induced further ubiquitination of the ORF3a protein (Figures 5C, S5G, and S5H). As a control, overexpression of the inactive mutant RNF5^{C42S}, whose ubiquitin-transferring ring finger domain is not functional,[55] did not induce ubiquitination of ORF3a (Figures S5I and S5J), which supports the hypothesis that RNF5 is a ubiquitin ligase for ORF3a. Additionally, we observed that RNF5 could not ubiquitinate other ER-anchored proteins such as SEC61B or other SARS-CoV-2 viral proteins such as ORF7b (Figure S5K). These results suggest that RNF5 is not a promiscuous ubiquitin ligase at the ER membrane and that ORF3a is a specific substrate of RNF5.

To verify whether ubiquitin ligase activity of RNF5 could interfere with the infectivity and viral replication of SARS-CoV-2 inside the host cell, A549-hACE2 cells[59] were transfected with mCherry-tagged functional RNF5 (mCherry-RNF5) or nonfunctional mutant RNF5^{C42S} (mCherry-RNF5^{C42S}) and mCherry (control) constructs, respectively, and then infected with an ancestral strain of live SARS-CoV-2 (Figures 5D, S6A–S6C). We found that the infection rates of SARS-CoV-2 in mCherry-RNF5-transfected cells (15.53%; 48 of 309) were lower than those in mCherry-transfected (24.20%; 38 of 157) or mCherry-RNF5^{C42S}-transfected cells (26.10%; 113 of 433) (Figure 5E; Data S3). To assess whether the decrease in the SARS-CoV-2 infection rate due to RNF5 overexpression could be replicated using other constructs, we measured the infection rates in A549-hACE2 cells transfected with hemagglutinin (HA)-tagged RNF5 constructs (Figures 5D, 5E, S6D, and S6E). We also observed that the infection rates of HA-RNF5-transfected cells (14.63%; 30 of 205) were lower than those of cells transfected with the inactive HA-RNF5^{C42S} (25%; 47 of 188), although this difference was not statistically significant ($p = 0.1018$; Figure 5E; Data S3). The nuclei counts, total transfection rate, infection rate in nontransfected cells, and total infection rate in all cells were comparable between the RNF5 and RNF5^{C42S} transfection conditions (Figures 5E and S6F; Data S3). Therefore, the lower infection rate of RNF5-transfected cells was likely driven by the functional ubiquitin ligase activity of RNF5. Notably, ORF3a expression was significantly lowered under mCherry-RNF5 expression than under mCherry and mCherry-RNF5^{C42S} expression (Figures 5F, 5G, and S6G). Therefore, RNF5 is responsible for ubiquitination that can be involved in the degradation pathway of ORF3a derived from SARS-CoV-2. Taken together, these results suggest that RNF5 interacts with SARS-CoV-2 proteins and potentially exerts anti-viral activity in the early phase of SARS-CoV-2 infection and replication inside host cells.

ORF3a expression affects RNF5 interactome

To investigate the RNF5 interactome, we used TurboID-RNF5 along with ORF3a using the *SR-PL* method. In the RNF5 interactome under both normal conditions and ORF3a overexpression, a remarkable proportion of biotin-labeled proteins were localized to the ER (Data S4 and S5) as RNF5 was localized at the ER membrane. In the basal state, proteins related to vesicle trafficking (i.e., ARF3, RAB29, and ACTN4) and protein degradation units (ZFAND5 and ZFAND6) were detected in the RNF5 interactome (Figure 6A). We further analyzed the RNF5 interactome using the *SR-PL* method under ORF3a expression (Figures 6B and 6C). Interestingly, we observed that other vesicle formation factors (i.e., EPS15, SAR1B, and ARL6IP5) were labeled with TurboID-RNF5 upon ORF3a expression ($\log_2$ fold change [$\log_2$FC] > 1.8, $-\log_{10}p > 1.5$), and it is likely that these protein factors are related to ORF3a-derived vesicle formation (Figures 2B, 2F, 5A, and 5B). Additionally, K186 of UBE2J1 was exclusively labeled with TurboID-RNF5 under ORF3a expression ($\log_2$FC: 1.26, $-\log_{10}p = 1.19$; Figure 6B; Data S4 and S5). Because UBE2J1 is characterized as an ER-anchored E2 ubiquitin-conjugating enzyme,[60] UBE2J1 may interact with and transfer ubiquitin to RNF5 at the ER membrane.

Notably, we exclusively observed biotin-labeled sites of EPS15 (K648), ANKLE2 (K262), and NDC1 (K416) by TurboID-RNF5 under ORF3a expression (Figure S7; Data S4 and S5), which showed other biotin-labeled site(s) by TurboID-RNF5 in the basal state: EPS15 (K754), ANKLE2

Figure 4. Identification of the ORF3a interactome and M interactome

(A) Subcellular distribution of the selected interactome of ORF3a (185 proteins) and M (226 proteins). See detailed information in Figure S4H and Data S1 and S2.

(B) Gene Ontology analysis (http://bioinformatics.sdstate.edu/go/) of ORF3a and M interactome. See detailed information in Figure S4I.

(C and D) Subcellular map of top 20 selected interactome of ORF3a (C) and M (D). Among the top 20 interactomes of ORF3a, 12 peptides overlapped with the mitochondrial-associated membrane (MAM) proteome[19] are shown as gray-colored shading.

(E) Flowchart showing the process of coloring principles of proposed membrane topologies and biotinylated sites of ORF3a and M's transmembrane interactomes.

(F) Proposed membrane topologies of the integral membrane proteins in ORF3a and M's interactome list, followed by (E). Biotin-labeled sites by TurboID-GBP were colored according to their samples (red: ORF3a; blue: M; purple: ORF3a and M). Proposed membrane topologies are shown in yellow. See detailed information in Figures S4J and S4K and Data S1 and S2.

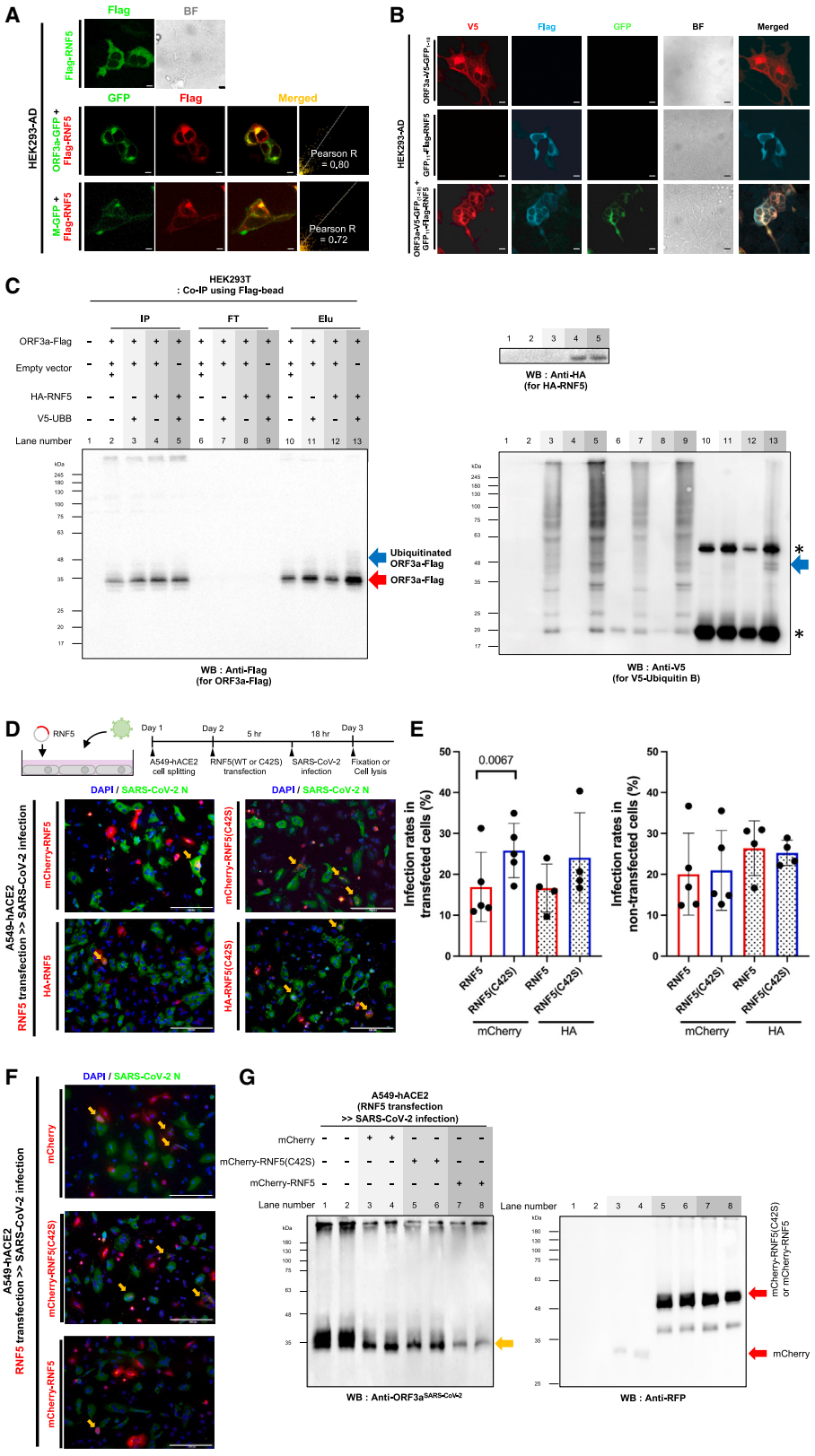

(legend on next page)

(K271, K546, K738, K759, and K883), and NDC1 (K430 and K437). Since the *in situ* biotinylation reaction is strictly regulated in a proximity-dependent manner, the exclusively biotin-labeled sites suggest that these sites are proximal to RNF5 under ORF3a expression. As the functions of these proteins are related to vesicle formation, it is intriguing to speculate whether the vesicles forming the RNF5 interactome exert the anti-viral function of RNF5 against SARS-CoV-2 infection inside host cells. However, further investigation is required to confirm this hypothesis.

Notably, UBE2J1, an E2 ubiquitin-conjugating enzyme, was found to be part of the RNF5 interactome upon ORF3a expression (Figure 6B). We hypothesized that UBE2J1 could be brought closer to RNF5 to increase its ubiquitination activity during ORF3a expression. We conducted a coIP analysis using ubiquitin as a bait protein, and the results showed that more UBE2J1 was eluted by ubiquitin under RNF5 expression, indicating that UBE2J1 strongly interacted with ubiquitin under RNF5 expression (Figure 6D). Using the AlphaFold multimer algorithm (AlphaFold v.2.3.0, https://github.com/deepmind/alphafold/blob/main/docs/technical_note_v2.3.0.md), we generated a virtual protein complex structure in which RNF5:UBE2J1∼UBB formed an E3:E2∼Ub complex with a low predicted alignment error (PAE) (Figures 6E and 6F). Along with our RNF5 interactome results, this model suggests that formation of the RNF5:UBE2J1∼UBB complex may be further induced by ORF3a expression, thereby increasing the ubiquitination activity of RNF5 (Figure 6G).

Construction of web-based search platform of ORF3a and M interactome

Furthermore, we built a user-accessible, web-based search platform showing detailed information about the ORF3a and M interactome obtained in this study (Figure 7A). This web-based platform is available at https://sarscov2.spatiomics.org. This site provides information on which protein was biotin labeled and at which lysine site in the biological triplicate samples of five cases (Figure 3A). If one entered the protein name or gene name of our findings, detailed biotin-labeled site information in each sample is presented (Figure 7B). Biotin-labeled site information is also summarized in the "summary" tab (Figure 7C). In a "heatmap" tab, raw mass signal intensity information of biotinylated peptides of the ORF3a and M interactome in all 15 samples are shown per the labeled protein. (Figure 7D). In the "iCn3D viewer" tab, we visualized the biotin-labeled sites on the protein structure based on the AlphaFold database using the iCn3D viewer algorithm (https://www.ncbi.nlm.nih.gov/Structure/icn3d/, Figure 7E). In this viewer, "red" represents ORF3a-specific sites, "blue" represents M-specific sites, and "pink" represents overlapped sites both in ORF3a- and M-specific sites over the controls. Furthermore, PubMed was linked to make it easier to access so that one can easily determine what kinds of studies exist on various topics (e.g., SARS-CoV-2) (Figure 7F). This web-based platform is continuously managed and updated to provide convenience of use. We believe that this user-friendly web database with an AlphaFold structure and virus-related literature links can be helpful in maximizing the utilization of our findings in future studies.

DISCUSSION

In our study, RNF5 was identified as part of the ORF3a interactome using *SR-PL*. The biotin-labeled K75 residue of RNF5 was exclusively and reproducibly shown in all triplicate samples of ORF3a:TurboID (Figure 3D; Data S1 and S2), whereas previously reported interactome mapping approaches, such as the conventional PL technique[13,14] and the AP method,[1,6] could not identify RNF5 in the ORF3a interactome, although their selections contained comparable or more findings. Our result is consistent with a previous study showing that several SARS-CoV-2 proteins, including ORF3a, are ubiquitinated in viral protein-expressing cells.[61] However, a recent study has highlighted the pro-viral role of RNF5 ubiquitination in a SARS-CoV-2 virion release assay.[62] In our study, we utilized hACE2-A549 cells to measure the SARS-CoV-2 infection rate, whereas another study utilized Vero-E6 cells to check the virion release rate. Thus, there is a possibility that RNF5 can work differentially in different cell types or can function as an anti-viral factor in the virus infection stage, and it can work as a pro-viral factor in the virion release stage. Additionally, we utilized N terminus-tagged RNF5, whereas the C terminus HA-tagged RNF5 was utilized in other studies. Since RNF5 is a tail-anchor TM protein with a C-terminal TM domain, we believe that the N-terminal RNF5 may interfere with its function at the ER membrane.

We hope that RNF5 and other interactome findings of this study will be useful for the development of anti-viral therapeutics

Figure 5. RNF5 ubiquitinates ORF3a of SARS-CoV-2

(A) Confocal microscopy images of FLAG-RNF5 with vPOI-GFP in HEK293-AD cells. BF, bright field. Scale bars: 10 μm. Additional results are shown in Figure S5B.

(B) Confocal microscopic images of ORF3a-V5-GFP_{1-10} or/and GFP_{11}-FLAG-RNF5 in HEK293-AD cells. Protein interaction-induced assembly of split GFP fragments (GFP_{1-10} and GFP_{11}) generates green fluorescence. BF, bright field, Scale bars: 10 μm. Additional results are shown in Figure S5D.

(C) Western blot analysis of ORF3a ubiquitination by RNF5 in HEK293T cells. Asterisks at 20 and 63 kDa in the anti-V5 blot result indicate eluted mouse immunoglobulin proteins. Additional blot results are shown in Figures S5E–S5H.

(D) Microscopy images of A549-hACE2 cells transfected with RNF5 constructs. Yellow-colored arrows showed transfected cells that were infected with SARS-CoV-2 (D and F). Scale bars: 200 μm. Additional imaging results are shown in Figures S6A–S6E.

(E) SARS-CoV-2 infection rates in A549-hACE2 cells overexpressing RNF5 compared with $RNF5^{C42S}$. See additional information in Figure S6F.

(F) Microscopy images of A549-hACE2 cells transfected with mCherry, mCherry-$RNF5^{C42S}$, and mCherry-RNF5. Scale bars: 200 μm.

(G) Western blot analysis of ORF3a expression level under mCherry, mCherry-$RNF5^{C42S}$, and mCherry-RNF5 expression followed by SARS-CoV-2 infection in A549-hACE2 cells. Expected size of ORF3a is presented with a yellow-colored arrow. Additional blot results are shown in Figure S6G.

(A and B) Representative data from one of two experiments. (C) Representative data from one of four experiments. (D and E) Data from five experiments (for mCherry) and four experiments (for HA). (E) Data are represented as mean ± SEM. (F and G) Representative data from one of two experiments.

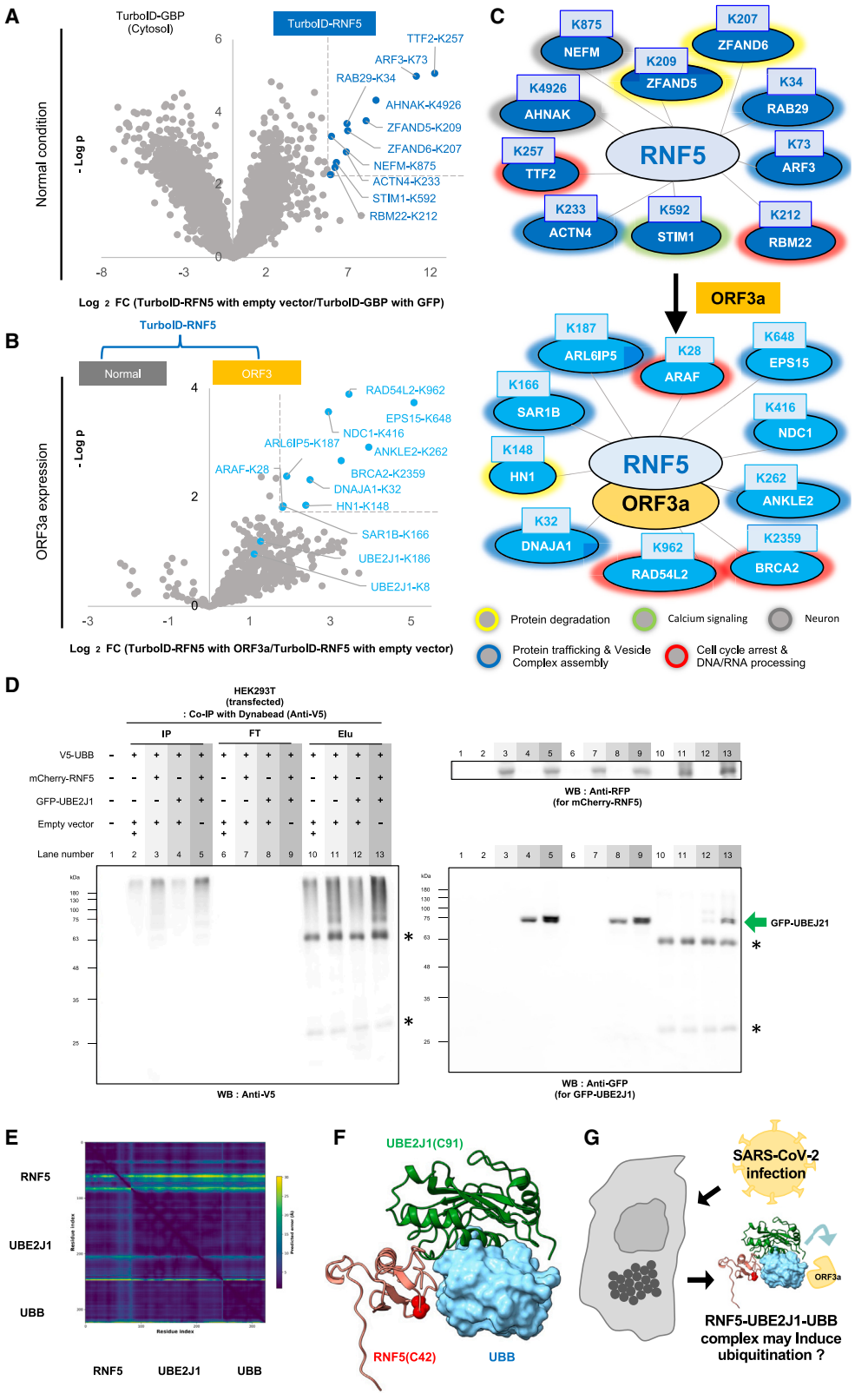

(legend on next page)

against SARS-CoV-2. Notably, many proteins in the ORF3a and M interactomes are already targeted by approved drug molecules (Tables S2 and S3), which may prove useful in designing drug-repurposing therapeutic strategies. As observed in other viruses that utilize the ER for replication,[63–66] including SARS-CoV,[67] our data showed that ORF3a and M largely affect the proteomic landscape in the ER. Recent reports have shown that the ectopic expression of ORF3a can hijack the HOPS complex and RAB7, which is identical in a full viral infection system. This event blocks the autophagosome-lysosome fusion process necessary for autolysosome formation.[2,68] We identified several lysosome-associated proteins in the ORF3a interactome, consistent with recent findings. In addition, we observed DMV structures in ORF3a-expressing cells, similar to those in SARS-CoV-2-infected cells.[38–40] As other vesicle formation machinery proteins were also shown in the RNF5 interactome, it is intriguing that ORF3a-induced membrane reorganization may activate antiviral host factors.

Based on these findings, we confirmed that our *SR-PL* workflow using the GFP/GBP system is an effective tool for interactome mapping of viral proteins in live cells. Since several viral proteins are initially cloned with GFP for imaging experiments typically performed in the initial stages of many virus studies, we expect that our TurboID-GBP could be an effective "plug-and-playable" component for rapid host interactome analysis with various GFP-tagged viral proteins without cloning additional constructs for PL experiments. This is especially relevant in situations where time is a constraint, such as during the COVID-19 pandemic.

Limitations of the study

First, as our experiment was conducted using the ectopic expression of SARS-CoV-2 viral proteins, it may not completely reflect the status of SARS-CoV-2 infection. The current recombinant SARS-CoV-2 viral RNA only allows genetic tagging within the ORF7 in the viral genome, implying that a strategy for genetic tagging of ORF3a or M in the viral genome has not yet been developed.[69] In the current situation, the ectopic expression of ORF3a and M with PL tags could be the best practical way to investigate the viral-host protein interactome (Table S4). In comparing our findings with previous SARS-CoV-2 viral interactome studies (e.g., PL[12–14,70] and AP-MS[1,6,71]), we observed a limited overlap in the results (Figure S8; Data S1). This discrepancy could be attributed to the variations in cell types, enrichment techniques, and analysis methods utilized across the studies (Table S4). Among these studies, our interactome analysis showed substantial overlap with the TurboID method by Zhang et al.,[12] as both studies utilized the same cell type and PL enzyme. Specifically, our study included 50% of the ORF3a interactome (3 out of 6 proteins) and 40% of the M interactome (16 out of 40 proteins) reported by Zhang et al.[12] Furthermore, it is worth mentioning that our current methodology successfully identified physiologically relevant interactions within the SARS-CoV-2 viral interactome, including the identification of RNF5. Notably, as RNF5 has also recently been characterized as an inducer of the degradation of other SARS-CoV-2 viral proteins, M[62] and E,[72] further investigation of the RNF5 recognition mechanism for these viral proteins might be intriguing.

STAR★METHODS

Detailed methods are provided in the online version of this paper and include the following:

- KEY RESOURCES TABLE
- RESOURCE AVAILABILITY
  - Lead contact
  - Materials availability
  - Data and code availability
- EXPERIMENTAL MODEL AND STUDY PARTICIPANT DETAILS
  - Cell lines
- METHOD DETAILS
  - Expression plasmids
  - Cell culture and transfections
  - Biotin labeling in live cells
  - Fluorescence microscope imaging
  - Co-immunoprecipitation of FLAG
  - Co-immunoprecipitation of V5
  - Immunoblotting
  - EM imaging and CLEM
  - Proteome digestion & enrichment of biotinylated peptides
  - Calculation of similarity value
  - LC-MS/MS analysis of enriched peptide samples
  - Processing LC-MS/MS dataset and identification of proteins
  - RNF5 plasmid transfection and virus infection
  - Immunofluorescence microscopy

Figure 6. Identification of the RNF5 interactome under ORF3a expression through the *SR-PL* method

(A) Enrichment by *SR-PL*-detected biotinylated peptides by TurboID-RNF5 against TurboID-GBP/GFP. x axis: log2 value of fold change of mass signal intensities; cutoff value is 5. y axis: −log10 value of p value; cutoff value is 2. See detailed information in Data S4 and S5 (A and B).

(B) Enrichment by *SR-PL*-detected biotinylated peptides by TurboID-RNF5 in samples of ORF3a-FLAG over an empty vector (control). x axis: log2 value of fold change of mass signal intensities; cutoff value is 1.8. y axis: −log10 value of p value; cutoff value is 1.5. UBE2J1, E2 ubiquitin-conjugating enzyme, is highlighted.

(C) Interaction partners of RNF5 under normal conditions and ORF3a expression. Biotinylated lysine sites are shown with gene names.

(D) Western blot analysis of GFP-UBE2J1 and mCherry-RNF5 by co-immunoprecipitation of V5-UBB co-expressed HEK293T cells. In anti-V5 and anti-GFP blot results, asterisks near the 25 and 63 kDa indicate eluted mouse immunoglobulin proteins from the mouse anti-V5 (or anti-GFP)-coated Dynabead.

(E) PAE (predicted alignment error) plot of AlphaFold multimer structure; RNF5(25–106)-UBE2J1(1–166)-UBB(1–76). In this plot, the bluer color indicates the lower PAE value that there is a higher accuracy of interaction between proteins.

(F) AlphaFold multimeric complex structure of RNF5(25–106)-UBE2J1(1–166)-UBB(1–76).

(G) The RNF5-UBE2J1-UBB complex may induce ubiquitination of host or viral proteins during SARS-CoV-2 infection.

(D) Representative data from one of three experiments.

A

UniProtID or Genename Search

SARS-CoV-2

B

SARS-CoV-2

Summary
Heatmap
iCn3D viewer
Eutils API PubMed search

C

CLCC1

Organism:	*Homo sapiens*
Protein name, UniProt:	Chloride channel CLIC-like protein 1 (Mid-1-related chloride channel protein 1)
Gene name, UniProt:	CLCC1
UniProt ID:	Q96S66
Localization, MitoAtlas:	non-mitochondrial
Localization, Uniprot:	Endoplasmic reticulum membrane ; Multi-pass membrane protein . Golgi apparatus membrane ; Multi-pass membrane protein . Nucleus membrane ; Multi-pass membrane protein . Note=Within the endoplasmic reticulum (ER), localizes to the mitochondria-associated ER membrane, a zone of contact between the
# of total TurboID labeled sites:	6
# of SARS-CoV-2 ORF3a specific sites:	4
positions of ORF3a specific sites:	K414, K470, K472 K518
# of SARS-CoV-2 M specific sites:	1
positions of M specific sites:	K472
Specific sites:	K414:SARS-CoV-2_ORF3a K437:inconclusive K463:inconclusive K470:SARS-CoV-2_ORF3a K472:SARS-CoV-2_ORF3a_AND_M K518:SARS-CoV-2_ORF3a

D

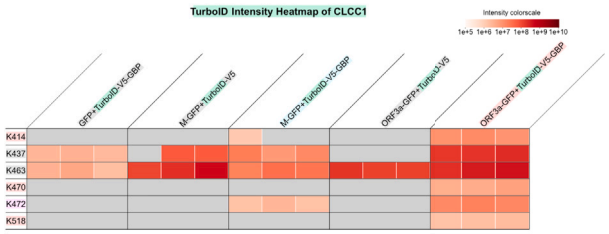

E

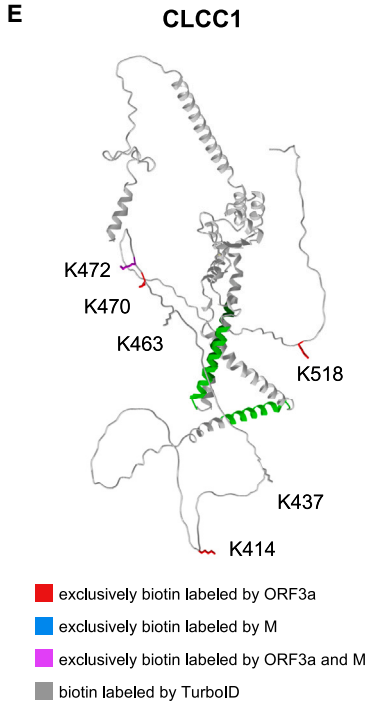

F

PubMed Query	Count	Link
CLCC1	15	Link
CLCC1 + SARS-CoV-2	1	Link
CLCC1 + SARS-CoV	1	Link
CLCC1 + virus	2	Link
CLCC1 + viral	1	Link
CLCC1 + membrane	3	Link

(legend on next page)

- Running AlphaFold2
- Data visualization
- Construction of web-based search platform of ORF3a and M interactome
- Transmembrane domain sources

- QUANTIFICATION AND STATISTICAL ANALYSIS

SUPPLEMENTAL INFORMATION

Supplemental information can be found online at https://doi.org/10.1016/j.celrep.2023.112835.

ACKNOWLEDGMENTS

This work was supported by the National Research Foundation of Korea (NRF-2020K1A3A1A47110634, NRF-2021K2A9A1A01102293, NRF-2022R1A2B5B03001658, NRF-2022M3H9A2096199, and 2022M3E5E8081185 to H.-W.R.; NRF-2022M3A9I2082294 and NRF-2021R1A2C2009336 to J.-S.K.; NRF-2022R1A2C1009376 to J.Y.M.); the Organelle Network Research Center (NRF-2017R1A5A1015366); and the Korea Health Industry Development Institute (KHIDI) funded by the Ministry of Health & Welfare and Ministry of Science and ICT, Republic of Korea (grant numbers: HU20C0204 and HU23C0204). H.-W.R. received support from the Samsung Science and Technology Foundation (SSTF-BA2201-08). J.Y.M. and M.J. were supported by the KBRI Basic Research Program through the Korea Brain Research Institute, funded by the Ministry of Science and ICT (Information & Communication Technology) (23-BR-01-03). A.S.-S. and J.K. were supported by a Sweden-South Korea collaborative grant from the Swedish Research Council (grant number: 2020-06312). The EM data were acquired from the Brain Research Core Facilities of KBRI. J.-S.K. was supported by the New Faculty Startup Fund from Seoul National University, Samsung Electronics (IO220819-02121-01), and the Institute for Basic Science of the Ministry of Science and ICT of Korea (IBS-R008-D1).

AUTHOR CONTRIBUTIONS

Y.-B.L., J.Y.M., J.-S.K., and H.-W.R. conceived the project. M.J. and J.Y.M. contributed to the EM imaging. J.K. and J.-S.K. performed the LC-MS/MS experiments and mass data processing. J.K. contributed to the construction of the web-based platform. M.-G.K. contributed to confocal imaging of Figure 1D. C.K. contributed to mass sample preparation. A.C., W.C., J.K., and A.S.-S. contributed to the experiments on live viral infection of transfected cells. All authors have written and edited the manuscript accordingly.

DECLARATION OF INTERESTS

A patent application related to the interactome findings was filed by Seoul National University.

Received: October 12, 2022
Revised: May 31, 2023
Accepted: July 5, 2023
Published: July 20, 2023

REFERENCES

1. Gordon, D.E., Jang, G.M., Bouhaddou, M., Xu, J., Obernier, K., White, K.M., O'Meara, M.J., Rezelj, V.V., Guo, J.Z., Swaney, D.L., et al. (2020). A SARS-CoV-2 protein interaction map reveals targets for drug repurposing. Nature *583*, 459–468. https://doi.org/10.1038/s41586-020-2286-9.
2. Zhang, Y., Sun, H., Pei, R., Mao, B., Zhao, Z., Li, H., Lin, Y., and Lu, K. (2021). The SARS-CoV-2 protein ORF3a inhibits fusion of autophagosomes with lysosomes. Cell Discov. *7*, 31. https://doi.org/10.1038/s41421-021-00268-z.
3. Konno, Y., Kimura, I., Uriu, K., Fukushi, M., Irie, T., Koyanagi, Y., Sauter, D., Gifford, R.J., USFQ-COVID19 Consortium; Nakagawa, S., and Sato, K. (2020). SARS-CoV-2 ORF3b Is a Potent Interferon Antagonist Whose Activity Is Increased by a Naturally Occurring Elongation Variant. Cell Rep. *32*, 108185. https://doi.org/10.1016/j.celrep.2020.108185.
4. Siu, K.L., Yuen, K.S., Castaño-Rodriguez, C., Ye, Z.W., Yeung, M.L., Fung, S.Y., Yuan, S., Chan, C.P., Yuen, K.Y., Enjuanes, L., and Jin, D.Y. (2019). Severe acute respiratory syndrome coronavirus ORF3a protein activates the NLRP3 inflammasome by promoting TRAF3-dependent ubiquitination of ASC. Faseb. J. *33*, 8865–8877. https://doi.org/10.1096/fj.201802418R.
5. Majumdar, P., and Niyogi, S. (2020). ORF3a mutation associated with higher mortality rate in SARS-CoV-2 infection. Epidemiol. Infect. *148*, e262. https://doi.org/10.1017/S0950268820002599.
6. Stukalov, A., Girault, V., Grass, V., Karayel, O., Bergant, V., Urban, C., Haas, D.A., Huang, Y., Oubraham, L., Wang, A., et al. (2021). Multilevel proteomics reveals host perturbations by SARS-CoV-2 and SARS-CoV. Nature *594*, 246–252. https://doi.org/10.1038/s41586-021-03493-4.
7. Rhee, H.W., Zou, P., Udeshi, N.D., Martell, J.D., Mootha, V.K., Carr, S.A., and Ting, A.Y. (2013). Proteomic mapping of mitochondria in living cells via spatially restricted enzymatic tagging. Science *339*, 1328–1331. https://doi.org/10.1126/science.1230593.
8. Roux, K.J., Kim, D.I., Raida, M., and Burke, B. (2012). A promiscuous biotin ligase fusion protein identifies proximal and interacting proteins in mammalian cells. J. Cell Biol. *196*, 801–810. https://doi.org/10.1083/jcb.201112098.
9. Branon, T.C., Bosch, J.A., Sanchez, A.D., Udeshi, N.D., Svinkina, T., Carr, S.A., Feldman, J.L., Perrimon, N., and Ting, A.Y. (2018). Efficient proximity labeling in living cells and organisms with TurboID. Nat. Biotechnol. *36*, 880–887. https://doi.org/10.1038/nbt.4201.
10. V'Kovski, P., Gerber, M., Kelly, J., Pfaender, S., Ebert, N., Braga Lagache, S., Simillion, C., Portmann, J., Stalder, H., Gaschen, V., et al. (2019). Determination of host proteins composing the microenvironment of coronavirus replicase complexes by proximity-labeling. Elife *8*, e42037. https://doi.org/10.7554/eLife.42037.
11. Chen, Z., Wang, C., Feng, X., Nie, L., Tang, M., Zhang, H., Xiong, Y., Swisher, S.K., Srivastava, M., and Chen, J. (2021). Interactomes of SARS-CoV-2 and human coronaviruses reveal host factors potentially affecting pathogenesis. EMBO J. *40*, e107776. https://doi.org/10.15252/embj.2021107776.
12. Zhang, Y., Shang, L., Zhang, J., Liu, Y., Jin, C., Zhao, Y., Lei, X., Wang, W., Xiao, X., Zhang, X., et al. (2022). An antibody-based

Figure 7. Outline of COVID interactome database

(A) Website frontpage layout (https://sarscov2.spatiomics.org).
(B) Website descriptions.
(C) The "summary" tab of search results for CLCC1.
(D) The "heatmap" tab of search results for CLCC1.
(E) The "iCn3D viewer" tab of search results for CLCC1. CLCC1 visualization of AlphaFold structure with the biotin-labeled proteins. TM domain is green colored and biotin-labeled sites are marked with blue, red, and purple colors according to its bait constructs.
(F) The "PubMed query" tab of search results for CLCC1. iCn3D: https://www.ncbi.nlm.nih.gov/Structure/icn3d/; UniProt: https://www.uniprot.org; DeepTMHMM: https://dtu.biolib.com/DeepTMHMM; TMbed: https://github.com/Rostlab/TMbed; AlphaFold: https://alphafold.ebi.ac.uk; and PubMed: https://pubmed.ncbi.nlm.nih.gov.

proximity labeling map reveals mechanisms of SARS-CoV-2 inhibition of antiviral immunity. Cell Chem. Biol. *29*, 5–18.e6. https://doi.org/10.1016/j.chembiol.2021.10.008.

13. Estelle, M.N.L., Yorgos, S., Anastassia, K., Jean-Pascal, G., Payman Samavarchi, T., Dae-Kyum, K., Hala, A., Marie, D., Patricia, C., Jennifer, J.K., et al. (2020). Global BioID-based SARS-CoV-2 proteins proximal interactome unveils novel ties between viral polypeptides and host factors involved in multiple COVID19-associated mechanisms. Preprint at bioRxiv. https://doi.org/10.1101/2020.08.28.272955.
14. Payman, S.-T., Hala, A., James, D.R.K., Audrey, A., Reuben, S., Zhen-Yuan, L., Dae-Kyum, K., Jennifer, J.K., Jonathan, S.-G., Christopher, D.G., et al. (2020). A SARS-CoV-2 – host proximity interactome. Preprint at bioRxiv. https://doi.org/10.1101/2020.09.03.282103.
15. Jonathan, R.S.-G., Audrey, A., Payman, S.-T., Hala, A., Vinitha, M., Dae-Kyum, K., Jennifer, J.K., Frederick, P.R., Anne-Claude, G., and Brian, R. (2020). A SARS-CoV-2 BioID-based virus-host membrane protein interactome and virus peptide compendium: new proteomics resources for COVID-19 research. Preprint at bioRxiv. https://doi.org/10.1101/2020.08.28.269175.
16. Lee, S.Y., Lee, H., Lee, H.K., Lee, S.W., Ha, S.C., Kwon, T., Seo, J.K., Lee, C., and Rhee, H.W. (2016). Proximity-Directed Labeling Reveals a New Rapamycin-Induced Heterodimer of FKBP25 and FRB in Live Cells. ACS Cent. Sci. *2*, 506–516. https://doi.org/10.1021/acscentsci.6b00137.
17. Udeshi, N.D., Pedram, K., Svinkina, T., Fereshetian, S., Myers, S.A., Aygun, O., Krug, K., Clauser, K., Ryan, D., Ast, T., et al. (2017). Antibodies to biotin enable large-scale detection of biotinylation sites on proteins. Nat. Methods *14*, 1167–1170. https://doi.org/10.1038/nmeth.4465.
18. Lee, S.Y., Kang, M.G., Shin, S., Kwak, C., Kwon, T., Seo, J.K., Kim, J.S., and Rhee, H.W. (2017). Architecture Mapping of the Inner Mitochondrial Membrane Proteome by Chemical Tools in Live Cells. J. Am. Chem. Soc. *139*, 3651–3662. https://doi.org/10.1021/jacs.6b10418.
19. Kwak, C., Shin, S., Park, J.S., Jung, M., Nhung, T.T.M., Kang, M.G., Lee, C., Kwon, T.H., Park, S.K., Mun, J.Y., et al. (2020). Contact-ID, a tool for profiling organelle contact sites, reveals regulatory proteins of mitochondrial-associated membrane formation. Proc. Natl. Acad. Sci. USA *117*, 12109–12120. https://doi.org/10.1073/pnas.1916584117.
20. Kim, K.E., Park, I., Kim, J., Kang, M.G., Choi, W.G., Shin, H., Kim, J.S., Rhee, H.W., and Suh, J.M. (2021). Dynamic tracking and identification of tissue-specific secretory proteins in the circulation of live mice. Nat. Commun. *12*, 5204. https://doi.org/10.1038/s41467-021-25546-y.
21. Van Haute, L., Lee, S.Y., McCann, B.J., Powell, C.A., Bansal, D., Vasiliauskaitė, L., Garone, C., Shin, S., Kim, J.S., Frye, M., et al. (2019). NSUN2 introduces 5-methylcytosines in mammalian mitochondrial tRNAs. Nucleic Acids Res. *47*, 8720–8733. https://doi.org/10.1093/nar/gkz559.
22. Park, J., Lee, S.Y., Jeong, H., Kang, M.G., Van Haute, L., Minczuk, M., Seo, J.K., Jun, Y., Myung, K., Rhee, H.W., and Lee, C. (2019). The structure of human EXD2 reveals a chimeric 3' to 5' exonuclease domain that discriminates substrates via metal coordination. Nucleic Acids Res. *47*, 7078–7093. https://doi.org/10.1093/nar/gkz454.
23. Ariotti, N., Hall, T.E., Rae, J., Ferguson, C., McMahon, K.A., Martel, N., Webb, R.E., Webb, R.I., Teasdale, R.D., and Parton, R.G. (2015). Modular Detection of GFP-Labeled Proteins for Rapid Screening by Electron Microscopy in Cells and Organisms. Dev. Cell *35*, 513–525. https://doi.org/10.1016/j.devcel.2015.10.016.
24. Xiong, Z., Lo, H.P., McMahon, K.A., Martel, N., Jones, A., Hill, M.M., Parton, R.G., and Hall, T.E. (2021). In vivo proteomic mapping through GFP-directed proximity-dependent biotin labelling in zebrafish. Elife *10*, e64631. https://doi.org/10.7554/eLife.64631.
25. Holzer, E., Rumpf-Kienzl, C., Falk, S., and Dammermann, A. (2022). A modified TurboID approach identifies tissue-specific centriolar components in C. elegans. PLoS Genet. *18*, e1010150. https://doi.org/10.1371/journal.pgen.1010150.
26. Anderson, P., and Kedersha, N. (2006). RNA granules. J. Cell Biol. *172*, 803–808. https://doi.org/10.1083/jcb.200512082.
27. Nover, L., Scharf, K.D., and Neumann, D. (1983). Formation of cytoplasmic heat shock granules in tomato cell cultures and leaves. Mol. Cell Biol. *3*, 1648–1655. https://doi.org/10.1128/mcb.3.9.1648-1655.1983.
28. Ren, Y., Shu, T., Wu, D., Mu, J., Wang, C., Huang, M., Han, Y., Zhang, X.Y., Zhou, W., Qiu, Y., and Zhou, X. (2020). The ORF3a protein of SARS-CoV-2 induces apoptosis in cells. Cell. Mol. Immunol. *17*, 881–883. https://doi.org/10.1038/s41423-020-0485-9.
29. Chan, C.M., Ma, C.W., Chan, W.Y., and Chan, H.Y.E. (2007). The SARS-Coronavirus Membrane protein induces apoptosis through modulating the Akt survival pathway. Arch. Biochem. Biophys. *459*, 197–207. https://doi.org/10.1016/j.abb.2007.01.012.
30. Fang, X., Gao, J., Zheng, H., Li, B., Kong, L., Zhang, Y., Wang, W., Zeng, Y., and Ye, L. (2007). The membrane protein of SARS-CoV suppresses NF-kappaB activation. J. Med. Virol. *79*, 1431–1439. https://doi.org/10.1002/jmv.20953.
31. Inoue, T., and Tsai, B. (2013). How viruses use the endoplasmic reticulum for entry, replication, and assembly. Cold Spring Harbor Perspect. Biol. *5*, a013250. https://doi.org/10.1101/cshperspect.a013250.
32. Freundt, E.C., Yu, L., Goldsmith, C.S., Welsh, S., Cheng, A., Yount, B., Liu, W., Frieman, M.B., Buchholz, U.J., Screaton, G.R., et al. (2010). The open reading frame 3a protein of severe acute respiratory syndrome-associated coronavirus promotes membrane rearrangement and cell death. J. Virol. *84*, 1097–1109. https://doi.org/10.1128/JVI.01662-09.
33. Mason, R.J. (2020). Pathogenesis of COVID-19 from a cell biology perspective. Eur. Respir. J. *55*, 2000607. https://doi.org/10.1183/13993003.00607-2020.
34. Martell, J.D., Deerinck, T.J., Sancak, Y., Poulos, T.L., Mootha, V.K., Sosinsky, G.E., Ellisman, M.H., and Ting, A.Y. (2012). Engineered ascorbate peroxidase as a genetically encoded reporter for electron microscopy. Nat. Biotechnol. *30*, 1143–1148. https://doi.org/10.1038/nbt.2375.
35. Deng, Y., and Angelova, A. (2021). Coronavirus-Induced Host Cubic Membranes and Lipid-Related Antiviral Therapies: A Focus on Bioactive Plasmalogens. Front. Cell Dev. Biol. *9*, 630242. https://doi.org/10.3389/fcell.2021.630242.
36. Snijder, E.J., Limpens, R.W.A.L., de Wilde, A.H., de Jong, A.W.M., Zevenhoven-Dobbe, J.C., Maier, H.J., Faas, F.F.G.A., Koster, A.J., and Bárcena, M. (2020). A unifying structural and functional model of the coronavirus replication organelle: Tracking down RNA synthesis. PLoS Biol. *18*, e3000715. https://doi.org/10.1371/journal.pbio.3000715.
37. Uchil, P.D., and Satchidanandam, V. (2003). Architecture of the flaviviral replication complex. Protease, nuclease, and detergents reveal encasement within double-layered membrane compartments. J. Biol. Chem. *278*, 24388–24398. https://doi.org/10.1074/jbc.M301717200.
38. Cortese, M., Lee, J.Y., Cerikan, B., Neufeldt, C.J., Oorschot, V.M.J., Köhrer, S., Hennies, J., Schieber, N.L., Ronchi, P., Mizzon, G., et al. (2020). Integrative Imaging Reveals SARS-CoV-2-Induced Reshaping of Subcellular Morphologies. Cell Host Microbe *28*, 853–866.e5. https://doi.org/10.1016/j.chom.2020.11.003.
39. Wolff, G., Limpens, R.W.A.L., Zevenhoven-Dobbe, J.C., Laugks, U., Zheng, S., de Jong, A.W.M., Koning, R.I., Agard, D.A., Grünewald, K., Koster, A.J., et al. (2020). A molecular pore spans the double membrane of the coronavirus replication organelle. Science *369*, 1395–1398. https://doi.org/10.1126/science.abd3629.
40. Klein, S., Cortese, M., Winter, S.L., Wachsmuth-Melm, M., Neufeldt, C.J., Cerikan, B., Stanifer, M.L., Boulant, S., Bartenschlager, R., and Chlanda, P. (2020). SARS-CoV-2 structure and replication characterized by in situ cryo-electron tomography. Nat. Commun. *11*, 5885. https://doi.org/10.1038/s41467-020-19619-7.
41. Nii, S., Morgan, C., Rose, H.M., and Hsu, K.C. (1968). Electron microscopy of herpes simplex virus. IV. Studies with ferritin-conjugated antibodies. J. Virol. *2*, 1172–1184. https://doi.org/10.1128/JVI.2.10.1172-1184.1968.

42. Schuck, S., Gallagher, C.M., and Walter, P. (2014). ER-phagy mediates selective degradation of endoplasmic reticulum independently of the core autophagy machinery. J. Cell Sci. *127*, 4078–4088. https://doi.org/10.1242/jcs.154716.

43. Snapp, E.L., Hegde, R.S., Francolini, M., Lombardo, F., Colombo, S., Pedrazzini, E., Borgese, N., and Lippincott-Schwartz, J. (2003). Formation of stacked ER cisternae by low affinity protein interactions. J. Cell Biol. *163*, 257–269. https://doi.org/10.1083/jcb.200306020.

44. Xie, L., Song, X.J., Liao, Z.F., Wu, B., Yang, J., Zhang, H., and Hong, J. (2019). Endoplasmic reticulum remodeling induced by Wheat yellow mosaic virus infection studied by transmission electron microscopy. Micron *120*, 80–90. https://doi.org/10.1016/j.micron.2019.01.007.

45. Fernández de Castro, I., Zamora, P.F., Ooms, L., Fernández, J.J., Lai, C.M.H., Mainou, B.A., Dermody, T.S., and Risco, C. (2014). Reovirus forms neo-organelles for progeny particle assembly within reorganized cell membranes. mBio *5*, e00931-13. https://doi.org/10.1128/mBio.00931-13.

46. Tenorio, R., Fernández de Castro, I., Knowlton, J.J., Zamora, P.F., Lee, C.H., Mainou, B.A., Dermody, T.S., and Risco, C. (2018). Reovirus sigmaNS and muNS Proteins Remodel the Endoplasmic Reticulum to Build Replication Neo-Organelles. mBio *9*, e01253-18. https://doi.org/10.1128/mBio.01253-18.

47. Davies, J.P., Almasy, K.M., McDonald, E.F., and Plate, L. (2020). Comparative multiplexed interactomics of SARS-CoV-2 and homologous coronavirus non-structural proteins identifies unique and shared host-cell dependencies. Preprint at bioRxiv. https://doi.org/10.1101/2020.07.13.201517.

48. Hamamoto, I., Nishimura, Y., Okamoto, T., Aizaki, H., Liu, M., Mori, Y., Abe, T., Suzuki, T., Lai, M.M.C., Miyamura, T., et al. (2005). Human VAP-B is involved in hepatitis C virus replication through interaction with NS5A and NS5B. J. Virol. *79*, 13473–13482. https://doi.org/10.1128/JVI.79.21.13473-13482.2005.

49. Chan, C.M., Tsoi, H., Chan, W.M., Zhai, S., Wong, C.O., Yao, X., Chan, W.Y., Tsui, S.K.W., and Chan, H.Y.E. (2009). The ion channel activity of the SARS-coronavirus 3a protein is linked to its pro-apoptotic function. Int. J. Biochem. Cell Biol. *41*, 2232–2239. https://doi.org/10.1016/j.biocel.2009.04.019.

50. Issa, E., Merhi, G., Panossian, B., Salloum, T., and Tokajian, S. (2020). SARS-CoV-2 and ORF3a: Nonsynonymous Mutations, Functional Domains, and Viral Pathogenesis. mSystems *5*, e00266-20. https://doi.org/10.1128/mSystems.00266-20.

51. Kern, D.M., Sorum, B., Mali, S.S., Hoel, C.M., Sridharan, S., Remis, J.P., Toso, D.B., Kotecha, A., Bautista, D.M., and Brohawn, S.G. (2021). Cryo-EM structure of SARS-CoV-2 ORF3a in lipid nanodiscs. Nat. Struct. Mol. Biol. *28*, 573–582. https://doi.org/10.1038/s41594-021-00619-0.

52. Miller, A.N., Houlihan, P.R., Matamala, E., Cabezas-Bratesco, D., Lee, G.Y., Cristofori-Armstrong, B., Dilan, T.L., Sanchez-Martinez, S., Matthies, D., Yan, R., et al. (2023). The SARS-CoV-2 accessory protein Orf3a is not an ion channel, but does interact with trafficking proteins. Elife *12*, e84477. https://doi.org/10.7554/eLife.84477.

53. Kuang, E., Okumura, C.Y.M., Sheffy-Levin, S., Varsano, T., Shu, V.C.W., Qi, J., Niesman, I.R., Yang, H.J., López-Otín, C., Yang, W.Y., et al. (2012). Regulation of ATG4B stability by RNF5 limits basal levels of autophagy and influences susceptibility to bacterial infection. PLoS Genet. *8*, e1003007. https://doi.org/10.1371/journal.pgen.1003007.

54. Li, Y., Tinoco, R., Elmén, L., Segota, I., Xian, Y., Fujita, Y., Sahu, A., Zarecki, R., Marie, K., Feng, Y., et al. (2019). Gut microbiota dependent anti-tumor immunity restricts melanoma growth in Rnf5(-/-) mice. Nat. Commun. *10*, 1492. https://doi.org/10.1038/s41467-019-09525-y.

55. Zhong, B., Zhang, L., Lei, C., Li, Y., Mao, A.P., Yang, Y., Wang, Y.Y., Zhang, X.L., and Shu, H.B. (2009). The ubiquitin ligase RNF5 regulates antiviral responses by mediating degradation of the adaptor protein MITA. Immunity *30*, 397–407. https://doi.org/10.1016/j.immuni.2009.01.008.

56. Zhong, B., Zhang, Y., Tan, B., Liu, T.T., Wang, Y.Y., and Shu, H.B. (2010). The E3 ubiquitin ligase RNF5 targets virus-induced signaling adaptor for ubiquitination and degradation. J. Immunol. *184*, 6249–6255. https://doi.org/10.4049/jimmunol.0903748.

57. Sun, Y., Zheng, H., Yu, S., Ding, Y., Wu, W., Mao, X., Liao, Y., Meng, C., Ur Rehman, Z., Tan, L., et al. (2019). Newcastle Disease Virus V Protein Degrades Mitochondrial Antiviral Signaling Protein To Inhibit Host Type I Interferon Production via E3 Ubiquitin Ligase RNF5. J. Virol. *93*, e00322-19. https://doi.org/10.1128/JVI.00322-19.

58. Luo, W.W., Li, S., Li, C., Zheng, Z.Q., Cao, P., Tong, Z., Lian, H., Wang, S.Y., Shu, H.B., and Wang, Y.Y. (2017). iRhom2 is essential for innate immunity to RNA virus by antagonizing ER- and mitochondria-associated degradation of VISA. PLoS Pathog. *13*, e1006693. https://doi.org/10.1371/journal.ppat.1006693.

59. Yang, J., Petitjean, S.J.L., Koehler, M., Zhang, Q., Dumitru, A.C., Chen, W., Derclaye, S., Vincent, S.P., Soumillion, P., and Alsteens, D. (2020). Molecular interaction and inhibition of SARS-CoV-2 binding to the ACE2 receptor. Nat. Commun. *11*, 4541. https://doi.org/10.1038/s41467-020-18319-6.

60. Cremer, T., Jongsma, M.L.M., Trulsson, F., Vertegaal, A.C.O., Neefjes, J., and Berlin, I. (2021). The ER-embedded UBE2J1/RNF26 ubiquitylation complex exerts spatiotemporal control over the endolysosomal pathway. Cell Rep. *34*, 108659. https://doi.org/10.1016/j.celrep.2020.108659.

61. Cao, Z., Xia, H., Rajsbaum, R., Xia, X., Wang, H., and Shi, P.Y. (2021). Ubiquitination of SARS-CoV-2 ORF7a promotes antagonism of interferon response. Cell. Mol. Immunol. *18*, 746–748. https://doi.org/10.1038/s41423-020-00603-6.

62. Yuan, Z., Hu, B., Xiao, H., Tan, X., Li, Y., Tang, K., Zhang, Y., Cai, K., and Ding, B. (2021). The E3 Ubiquitin Ligase RNF5 Facilitates SARS-CoV-2 Membrane Protein-Mediated Virion Release. mBio *13*, e0316821. https://doi.org/10.1128/mbio.03168-21.

63. Zou, D., Xu, J., Duan, X., Xu, X., Li, P., Cheng, L., Zheng, L., Li, X., Zhang, Y., Wang, X., et al. (2019). Porcine epidemic diarrhea virus ORF3 protein causes endoplasmic reticulum stress to facilitate autophagy. Vet. Microbiol. *235*, 209–219. https://doi.org/10.1016/j.vetmic.2019.07.005.

64. Monel, B., Compton, A.A., Bruel, T., Amraoui, S., Burlaud-Gaillard, J., Roy, N., Guivel-Benhassine, F., Porrot, F., Génin, P., Meertens, L., et al. (2017). Zika virus induces massive cytoplasmic vacuolization and paraptosis-like death in infected cells. EMBO J. *36*, 1653–1668. https://doi.org/10.15252/embj.201695597.

65. Wang, K., Lu, W., Chen, J., Xie, S., Shi, H., Hsu, H., Yu, W., Xu, K., Bian, C., Fischer, W.B., et al. (2012). PEDV ORF3 encodes an ion channel protein and regulates virus production. FEBS Lett. *586*, 384–391. https://doi.org/10.1016/j.febslet.2012.01.005.

66. Lee, Y.R., Kuo, S.H., Lin, C.Y., Fu, P.J., Lin, Y.S., Yeh, T.M., and Liu, H.S. (2018). Dengue virus-induced ER stress is required for autophagy activation, viral replication, and pathogenesis both in vitro and in vivo. Sci. Rep. *8*, 489. https://doi.org/10.1038/s41598-017-18909-3.

67. Fung, T.S., Huang, M., and Liu, D.X. (2014). Coronavirus-induced ER stress response and its involvement in regulation of coronavirus-host interactions. Virus Res. *194*, 110–123. https://doi.org/10.1016/j.virusres.2014.09.016.

68. Miao, G., Zhao, H., Li, Y., Ji, M., Chen, Y., Shi, Y., Bi, Y., Wang, P., and Zhang, H. (2021). ORF3a of the COVID-19 virus SARS-CoV-2 blocks HOPS complex-mediated assembly of the SNARE complex required for autolysosome formation. Dev. Cell *56*, 427–442.e5. https://doi.org/10.1016/j.devcel.2020.12.010.

69. Hou, Y.J., Okuda, K., Edwards, C.E., Martinez, D.R., Asakura, T., Dinnon, K.H., 3rd, Kato, T., Lee, R.E., Yount, B.L., Mascenik, T.M., et al. (2020). SARS-CoV-2 Reverse Genetics Reveals a Variable Infection Gradient in the Respiratory Tract. Cell *182*, 429–446.e14. https://doi.org/10.1016/j.cell.2020.05.042.

70. May, D.G., Martin-Sancho, L., Anschau, V., Liu, S., Chrisopulos, R.J., Scott, K.L., Halfmann, C.T., Diaz Pena, R., Pratt, D., Campos, A.R., and Roux, K.J. (2022). A BioID-Derived Proximity Interactome for SARS-CoV-2 Proteins. Viruses *14*. https://doi.org/10.3390/v14030611.

71. Zhou, Y., Liu, Y., Gupta, S., Paramo, M.I., Hou, Y., Mao, C., Luo, Y., Judd, J., Wierbowski, S., Bertolotti, M., et al. (2023). A comprehensive SARS-CoV-2-human protein-protein interactome reveals COVID-19 pathobiology and potential host therapeutic targets. Nat. Biotechnol. *41*, 128–139. https://doi.org/10.1038/s41587-022-01474-0.

72. Li, Z., Hao, P., Zhao, Z., Gao, W., Huan, C., Li, L., Chen, X., Wang, H., Jin, N., Luo, Z.Q., et al. (2023). The E3 ligase RNF5 restricts SARS-CoV-2 replication by targeting its envelope protein for degradation. Signal Transduct. Target. Ther. *8*, 53. https://doi.org/10.1038/s41392-023-01335-5.

73. Ziegler, T., Matikainen, S., Rönkkö, E., Osterlund, P., Sillanpää, M., Sirén, J., Fagerlund, R., Immonen, M., Melén, K., and Julkunen, I. (2005). Severe acute respiratory syndrome coronavirus fails to activate cytokine-mediated innate immune responses in cultured human monocyte-derived dendritic cells. J. Virol. *79*, 13800–13805. https://doi.org/10.1128/JVI.79.21.13800-13805.2005.

STAR★METHODS

KEY RESOURCES TABLE

REAGENT or RESOURCE	SOURCE	IDENTIFIER
Antibodies		
V5 Tag Monoclonal Antibody (mouse)	Invitrogen	#R960-25
GFP Monoclonal Antibody (mouse)	Invitrogen	#MA5-15256
Anti-StrepMAB-Classic, purified, lyophilized, (mouse)	IBA	#2-1597-001
HA Tag Polyclonal Antibody	Thermofisher	#71-5500
FLAG rabbit Polyclonal Antibody	Sigma Aldrich	#F7425
Ubiquitin Antibody	Santa Cruz biotechnology	#SC-166553
Calnexin Antibody	Santa Cruz biotechnology	#SC-23954
RFP rabbit Antibody	Abcam	#ab34771
SARS-CoV-2 ORF3a polyclonal antibody anti-ORF3a	Thermofisher	#PA5116946
Alexa Fluor 568 IgG rabbit	Invitrogen	#A11011
Alexa Fluor 568 IgG mouse	Invitrogen	#A11004
Alexa Fluor 647 IgG rabbit	Invitrogen	#A21245
Streptavidin, Alexa Fluor 647 conjugate	Invitrogen	#S21374
Goat Anti-Mouse IgG (H + L)-HRP conjugate	Bio-rad	#1706516
Anti-rabbit IgG, HRP-linked Antibody	Cell signaling	#7074S
Streptavidin-HRP	Thermofisher	#21126
Chemicals, peptides, and recombinant proteins		
Anti-Flag affinity gel beads	Bimaker	#B23102
Dynabeads Protein G	Invitrogen	#10004D
4% paraformaldehyde	CHEMBIO	#CBPF-9004
HyClone Dulbecco's Modified Eagle Medium (DMEM) with high glucose: Liquid	Cytiva	#SH30022.01
FBS	Atlas Biologicals	#EF-0500-A
RIPA lysis buffer	ELPISBIO	#EBA-1149
Protease inhibitor cocktail	Invitrogen	#78438
biotin	Alfa aesar	#A14207
Sodium azide	Alfa aesar	#14314
Sodium ascorbate	Sigma Aldrich	#A4034
Trolox	Sigma Aldrich	#238813
Urea	Sigma Aldrich	#U5378
20X TBS	Thermofisher	#28358
Acetone	Sigma Aldrich	#650501
Ammonium bicarbonate	Sigma Aldrich	#A6141
Sodium dodecyl sulfate	Sigma Aldrich	#436143
TPCK-Trypsin	Thermofisher	#20233
Dithiothreitol	Sigma Aldrich	#43819
Iodoacetoamide	Sigma Aldrich	#I1149
Trifluoroacetic acid	Sigma Aldrich	#T6508-10AMP
Formic acid	Thermofisher	#28905
Streptavidin-coated magnetic beads	Pierce	#88817
Glutaraldehyde	Electron Microscopy Sciences	#16200
Paraformaldehyde	Electron Microscopy Sciences	#19210
Osmium tetroxide	Electron Microscopy Sciences	#19150
DAB	Sigma Aldrich	#D8001

(*Continued on next page*)

Continued

REAGENT or RESOURCE	SOURCE	IDENTIFIER
Uranyl acetate	Electron Microscopy Sciences	#22400
EMBed-812 embedding kit	Electron Microscopy Sciences	#14120
Uranyless	Electron Microscopy Sciences	#22409
Lead citrate	Electron Microscopy Sciences	#22410
Deposited data		
DOI number of Mendeley data	https://doi.org/10.17632/wxy2fkp5w8.1	This paper
ORF3a and M interactome	ProteomeXchange Consortium (accession no. PXD041368)	This paper
RNF5 interactome under ORF3a expression	ProteomeXchange Consortium (accession no. PXD032032)	This paper
Experimental models: Cell lines		
HEK293	Gift from Professor Kim H. at the Ulsan National Institute of Science and Technology (Korea)	N/A
HEK293T	Gift from Professor Kim H. at the Ulsan National Institute of Science and Technology (Korea)	N/A
Cos7	Gift from Professor Kim H. at the Ulsan National Institute of Science and Technology (Korea)	N/A
HeLa	Dr. Mun at the Korea Brain Research Institute (Korea)	N/A
A549	Dr. Mun at the Korea Brain Research Institute (Korea)	N/A
A549-hACE2	Gift from Oscar Fernandez-Capetillo at the Science for Life Lab (Sweden)	N/A
Software and algorithms		
AlphaFold v2.3.0	dockerized software under Linux (Ubuntu 22, AMD Ryzen 9 5950X, 128 GB RAM, NVidia RTX 4090 with 24GB RAM)	N/A
GraphPad Prism 9	GraphPad software	N/A
LAS X	LAS X software	N/A
ImageJ	NIH	N/A
PhotoZoom Pro 8 software	Benvista Ltd., Houston, TX, USA	N/A
Other		
Speed-vac	HyperCOOL	HC3110
Thermomixer	Thermofisher	N/A
TEM (Tecnai G2)	FEI	N/A
Confocal microscope (Nikon A1 RSi/Ti-E)	Nikon	N/A
Ultramicrotome (UC7)	Leica	N/A

RESOURCE AVAILABILITY

Lead contact

Further information and requests for resources and reagents should be directed to and will be fulfilled by the lead contact, Hyun-Woo Rhee (rheehw@snu.ac.kr).

Materials availability

Plasmids generated in this study are available from the lead contact with a completed materials transfer agreement. This study did not generate new unique reagents.

Data and code availability

- The raw LC-MS data generated in this study were deposited in the ProteomeXchange Consortium. The ORF3a and M interactome (accession no. PXD041368; username: reviewer_pxd041368@ebi.ac.uk; password:0IvSa1PG). The RNF5 interactome during ORF3a expression (accession no. PXD032032, User name: reviewer_pxd032032@ebi.ac.uk, Password: GoPAnSPk).
- This paper does not report original code.

- Any additional information required to reanalyze the data reported in this work paper is available from the lead contact upon request.

EXPERIMENTAL MODEL AND STUDY PARTICIPANT DETAILS

Cell lines

HEK293, HEK293T, and Cos7 cells were gifts from Professor Kim H. at the Ulsan National Institute of Science and Technology (Korea). HeLa and A549 cells were acquired from Dr. Mun at the Korea Brain Research Institute (Korea). A549 cells expressing hACE2 were kindly gifted by Oscar Fernandez-Capetillo at the Science for Life Lab (Sweden). The cell lines were cultured according to the manufacturer's instructions.

METHOD DETAILS

Expression plasmids

Genes with epitope tags (V5, FLAG, HA, twin strep) were cloned into pCDNA3, pCDNA3.1, and pCDNA5 by digestion with enzymatic restriction sites and ligation with T4 DNA ligase. After simultaneously digesting the PCR products and cutting the vectors, they were ligated. CMV promoter enables gene expression in mammalian cells. Table S1 summarizes information on these constructs. Templates for SARS-CoV-2 were obtained from Professors Kim Ho Min (KAIST) and V. Narry Kim (SNU Biology).

Cell culture and transfections

The morphology and confluence of cells were examined under a microscope. The cells were incubated in Dulbecco's modified Eagle's medium (Cytiva, cat. No., SH30022.01) supplemented with 10% fetal bovine serum (Atlas Biologicals, cat. No., EF-0500-A) in a 37°C incubator 5% CO_2 (v/v). Genes were introduced into the cells using PEI at 60–80% confluence. For 12-well-plate scale experiments, we transfected a total of 1000 ng plasmid DNA. For the co-transfection of two or three plasmids, 500 ng or 333 ng of plasmid DNA was transfected. For large-scale experiments in 6-well plates, T25 flasks, or T75 flasks, we transfected 2000, 5000, or 15000 ng of plasmid DNA, respectively.

Biotin labeling in live cells

Using a transient transfection reagent, PEI genes including TurboID were introduced into HEK293-AD, HEK293, or HEK293T cells. After 16–24 h, the medium was changed to 500 μL (24 well plate) or 1 mL (12 well plate) fresh growth medium containing 50 μM biotin (Alfa Aesar, cat. No., A14207). These cells were incubated at 37°C and 5% CO_2 for 30 min for using TurboID in accordance with the previously published protocols. The reaction was terminated by two washes with Dulbecco's phosphate-buffered saline (DPBS). Lysis was performed for Western blot analysis or mass sampling, and fixation was performed for fluorescence microscopy.

Fluorescence microscope imaging

Cells were split on coverslips (thickness no. 1.5, radius:18 mm) on 12-well plates (0.5 × 10^6 cells) for microscopy imaging. vPOI-GFP-expressing cells were fixed in 4% paraformaldehyde solution (CHEMBIO, cat. No., CBPF-9004) at room temperature for 10–15 min. Cells were washed twice with Dulbecco's phosphate-buffered saline (DPBS). To detect vPOI-GFP expression, washed cells were maintained in DPBS on 4°C refrigerator for imaging by Leica (NICEM in Seoul National University, Korea) with objective lens (HC PL APO 100×/1.40 OIL), White Light Laser (WLL, 470–670 nm, 1 nm tunable laser), HyD detector and controlled by LAS X software.

Co-expressing or biotin-labeled cells were fixed with a 4% paraformaldehyde solution (CHEMBIO, cat. No., CBPF-9004) in DPBS at room temperature for 10–15 min. Cells were then washed with DPBS, two times, and permeabilized with cold methanol at −20°C for 10 min. Cells were washed again, two times, with DPBS and blocked for 30 min with 2% BSA in DPBS at room temperature (25°C). To detect expression or biotinylation patterns, primary antibodies, such as anti-V5 (Invitrogen, cat. No., R960-25; 1:5,000 dilution) for 1 h at room temperature. After two washes with TBST, the cells were simultaneously incubated with a secondary Alexa Fluor 568 IgG mouse antibody (Molecular Probes, cat. No., A11004, 1:1,000 dilution) and Streptavidin, Alexa Fluor 647 conjugate (Invitrogen, cat. No. S21374, 1:1,000 dilution) for 30 min at room temperature. Cells were then washed two times with TBST and maintained in DPBS at 4°C for imaging using Leica (NICEM in Seoul National University, Korea). Pearson's correlation was conducted using the ImageJ software (NIH).

Co-immunoprecipitation of FLAG

The constructs were then transfected with PEI. After 16 h, the samples were lysed using RIPA buffer (ELPISBIO, cat. No., EBA-1149) containing 1× protease inhibitor cocktail (Invitrogen, cat. No., 78438) for 10 min at room temperature. After transferring the lysates to e-tubes, the samples were vortexed for 2–3 min at room temperature. After centrifugation at 15,000 × *g* for 10 min at 4°C, supernatant was collected. The samples were incubated with washed anti-FLAG affinity gel beads (Bimaker, cat. No., B23102) for 2 h at 4°C. Then they were washed more than three times and eluted using 1× SDS-PAGE loading buffer at 95°C for 5 min.

Co-immunoprecipitation of V5

The constructs were then transfected with PEI. After 16 h, the samples were lysed using RIPA buffer (ELPISBIO, cat. No., EBA-1149) containing 1× protease inhibitor cocktail (Invitrogen, cat. No., 78438) for 10 min at room temperature. After transferring the lysates to e-tubes, the samples were vortexed for 2–3 min at room temperature. After centrifugation at 15,000 × g for 10 min at 4°C, the supernatant was collected. Anti-V5 antibody (cat. No. R960-25) was incubated with Dynabeads Protein G (Invitrogen, cat. No., 10004D) for 1 h at RT. They were then washed more than three times and incubated with supernatants containing proteins for 1 h at RT. Then they were washed more than three times and eluted using 1× SDS-PAGE loading buffer at 95°C for 5 min.

Immunoblotting

12-well plates (0.5 × 10^6 cells) and 6-well plates (1.2 × 10^6 cells) were used for Western blot analysis. Transfected and biotinylated cell samples were lysed using RIPA buffer (ELPISBIO; cat. No., EBA-1149) containing 1× protease inhibitor cocktail (Invitrogen, cat. No., 78438) for 10 min at room temperature. After transferring the lysates to e-tubes, the samples were vortexed for 2–3 min at room temperature. Using centrifugation at 15,000 × *g* for 10 min at 4°C, samples were clarified. They were boiled in 1× SDS-PAGE loading buffer at 95°C for 5 min. After resolving the protein samples by SDS-PAGE and transferring the protein samples to a membrane, immunoblotting analysis was performed using antibodies. The membranes were blocked for 30 min with a 2% skim milk solution at room temperature. After washing three times with TBST for 5 min each at room temperature, primary antibodies, namely anti-V5 (Invitrogen, cat. No., R960-25, 1:10,000 dilution), anti-GFP (Invitrogen, cat. No., MA5-15256, 1:3,000 dilution), anti-HA (ThermoFisher, cat. No., 71–5500, 1:10,000 dilution), anti-FLAG (Sigma Aldrich, cat. No., F7425, 1:10,000 dilution), anti-RFP (abcam, cat. No., ab34771), anti-ORF3a (ThermoFisher cat. No., PA5116946) and anti-Strep (IBA, cat. No., 2-1597-001, 1:1,000 dilution), was incubated for 16 h at 4°C. After washing thrice with TBST for 5 min at room temperature, secondary antibodies, namely mouse-HRP (Bio-Rad, cat. No., 1706516, 1:3,000 dilution), and rabbit-HRP (Cell Signaling, cat. No., 7074S, 1:3,000 dilution) or SA-HRP (Thermo Fisher, cat. No., 21126, 1:10,000 dilution) was incubated for 1 h at room temperature. After washing three times with TBST for 5 min at room temperature, the results of the immunoblotting assay were obtained using ECL solution and the GENESYS program. Line-scan analysis was performed using the ImageJ software (NIH). After subtracting the intensity value at the background, protein bands from top to bottom of each lane were plotted as the x axis, and the intensity of bands from top to bottom of each lane was plotted as the y axis.

EM imaging and CLEM

To observe the DAB-stained cells, the cells were cultured in 35-mm glass grid-bottomed culture dishes (MatTek Life Sciences, MA, USA) to 30–40% confluency (5 × 10^4 cells). The cells were transfected with DNA plasmids using Lipofectamine 2000 (Life Technologies, Carlsbad, CA, USA). The next day, the cells were fixed with 1% glutaraldehyde (Electron Microscopy Sciences, cat. No., 16200) and 1% paraformaldehyde (Electron Microscopy Sciences, cat. No., 19210) in 0.1 M cacodylate solution (pH 7.0) for 1 h at 4°C. After washing, a 20 mM glycine solution was used to quench the unreacted aldehyde. DAB staining (Sigma, cat. No., D8001) took approximately 20–40 min until a light-brown stain was visible under an inverted light microscope. DAB-stained cells were post-fixed with 2% osmium tetroxide in distilled water for 30 min at 4°C and *en bloc* in 1% uranyl acetate (EMS, USA, cat. No., 22400) overnight and dehydrated using a graded ethanol series. Samples were embedded using an EMBed-812 embedding kit (Electron Microscopy Sciences, USA, cat. No., 14120) and polymerized in oven at 60°C. Polymerized samples were sectioned (60 nm) using an ultramicrotome (UC7; Leica Microsystems, Germany), and mounted on copper slot grids with a specimen support film. Sections were stained with UranyLess (Electron Microscopy Sciences, cat. No., 22409) and lead citrate (Electron Microscopy Scieneces, cat. No., 22410) and viewed using a Tecnai G2 transmission electron microscope (Thermo Fisher Scientific, USA).

For CLEM observation, the ORF3a-GFP-, M-mCherry-, and M-GFP-transfected cells were imaged under a confocal light microscope (Ti-RCP, Nikon, Japan) in living cells, and cells were fixed with 1% glutaraldehyde and 1% paraformaldehyde in 0.1 M cacodylate solution (pH 7.0). After washing, the cells were dehydrated using a graded ethanol series and infiltrated with the embedding medium. Following embedment, 60 nm sections were cut horizontally to the plane of the block (UC7; Leica Microsystems, Germany) and mounted on copper slot grids with a specimen support film. The sections were then stained with uranyl acetate and lead citrate. Cells were observed at 120 kV using a Tecnai G2 microscope (Thermo Fisher Scientific). Confocal micrographs were produced as high-quality large images using the PhotoZoom Pro 8 software (Benvista Ltd., Houston, TX, USA). Enlarged fluorescence images were fitted to the electron micrographs using the ImageJ BigWarp program.

Proteome digestion & enrichment of biotinylated peptides

For mass sampling, HEK293T cells were split into three T75 flasks (8.4 × 10^6 cells from each T75 flask) for triplicate samples per condition. For two transiently co-expressed constructs, vPOI-GFP and TurboID-GBP (or TurboID-RNF5 and ORF3a-Flag), the cells were grown to 70–80% confluence and transfected with the desired constructs using PEI. After 16 h (transfection), 50 μM biotin (Alfa aesar, cat. No., A14207) were treated for 30 min in a 37°C incubator. After biotin labeling, the cells were washed 3–4 times with cold DPBS and lysed with 1.5 mL 2% SDS in 1× TBS (25 mM Tris, 0.15 M NaCl, pH 7.2, Thermo Scientific, cat. No., 28358) containing a 1× protease inhibitor cocktail. These lysates underwent ultrasonication (Bioruptor, diagenode) 3–4 times for 15 min in a cold room. For removing free biotin, 5–6 times the sample volume of cold acetone stored at −20°C (Sigma Aldrich, cat. No., 650501) was mixed with lysates and stored at −20°C for at least 2 h. The samples were centrifuged at 13,000 × *g* for 10 min at

4°C. The supernatant was discarded gently. Cold acetone, 6.3 mL, and 700 μL of 1× TBS were mixed with the pellet. These mixtures were then vigorously vortexed and stored at −20°C for at least 2 h or overnight. The samples were then centrifuged at 13,000 × *g* for an additional 10 min at 4°C. The supernatant was discarded gently. After the pellet had dried naturally for 3–5 min, it was resolubilized with 1 mL of 8 M urea (Sigma-Aldrich, cat. No., U5378) in 50 mM ammonium bicarbonate (ABC, Sigma Aldrich, cat. No., A16141). Protein concentrations were calculated using bicinchoninic acid assay. Samples were vortexed at 650 rpm for 1 h at 37°C using thermomixer (Eppendorf) for denaturation. The samples were reduced with 10 mM dithiothreitol (Sigma-Aldrich, cat. No., 43816) at 650 rpm for 1 h at 37°C using Thermomixer (Eppendorf), while samples alkylation was accomplished in 40 mM iodoacetoamide (Sigma-Aldrich, cat. No., I1149) at 650 rpm for 1 h at 37°C using thermomixer (Eppendorf). The samples were diluted eight times with 50 mM ABC (Sigma-Aldrich, cat. No., A16141). mM of $CaCl_2$ (Alfa Aesar; cat. No., 12312) was added to a final concentration of 1 mM. Samples were digested with trypsin (ThermoFisher, cat. No., 20233) (50:1 w/w) at 650 rpm for 6–18 h at 37°C using thermomixer (Eppendorf). The insoluble materials were removed by centrifugation for 3 min at 10,000 × *g*. Streptavidin beads (300 μL; Pierce, cat. No. 88817) were washed three to four times using 2 M urea in 1× TBS for 3–4 times, were then added to the samples, and then rotated for 1 h at room temperature. The flow-through fraction was not discarded, and the beads were washed 2–3 times with 2 M urea in 50 mM ABC. After removing the supernatant, the beads were washed with pure water and transferred to new tubes. After adding 500 μL 80% acetonitrile (Sigma Aldrich, cat. No., 900667), and 0.2% TFA (Sigma-Aldrich, cat. No., T6508) and 0.1% formic acid (FA; Thermo Scientific, cat. No., 28905), heat such biotinylated peptides at 60°C and mixed at 650 rpm. The supernatant without streptavidin beads was transferred to new tubes. This elution step was repeated at least four times. The total eluted fractions were dried for 5 h using a Speed-Vac (Eppendorf). Before samples were injected to MS, they were stored at −20°C.

Calculation of similarity value

The similarity value for each mass sample was calculated as described previously. The correlation index C_{ij} is introduced to calculate the similarity value. The following Equation shows the calculation of the similarity value.

$$C_{ij} = \frac{\frac{1}{N}\sum_{k=1}^{N} I_i(k) I_j(k)}{\sqrt{\frac{1}{N}\sum_{k=1}^{N} I_i(k)^2}\sqrt{\frac{1}{N}\sum_{k=1}^{N} I_j(k)^2}}$$

As a result of C_{ij} ranging from 0 to 1, a larger value indicates more similarity, whereas a smaller value indicates less similarity.

LC-MS/MS analysis of enriched peptide samples

Analytical capillary columns (100 cm × 75 μm i.d.) and trap columns were packed in-house with 3 m Jupiter C18 particles (Phenomenex, Torrance). The long analytical column was placed in a column heater (Analytical Sales and Services) regulated to a temperature of 45°C. A NanoAcquity UPLC system (Waters) was operated at a flow rate of 300 nL/min for 2 h with a linear gradient ranging from 95% solvent A (H_2O with 0.1% formic acid) to 40% solvent B (acetonitrile with 0.1% formic acid). The enriched samples were analyzed using an Orbitrap Fusion Lumos mass spectrometer (Thermo Scientific) equipped with an in-house customized nanoelectrospray ion source. Precursor ions were acquired (m/z 300–1,500) at 120 K resolving power, and isolation of the precursor for MS/MS analysis was conducted with a 1.4 Th. High-energy collisional dissociation (HCD) with 30% collision energy was used for sequencing, with an automatic gain control (AGC) target of 1E5. The resolving power for the acquired MS2 spectra was set to 30 k at a maximum injection time of 200 ms.

Processing LC-MS/MS dataset and identification of proteins

All MS/MS data were searched using MaxQuant (version 1.5.3.30) with Andromeda search engine at 10 and 20 ppm mass tolerance for precursor and fragment ions, respectively, against the SwissProt *Homo sapiens* proteome database (2020.01 ver., 20,199 entries, UniProt (http://www.uniprot.org/)). Label-free quantification (LFQ) and matching between runs were performed using the following search parameters: semi-tryptic digestion, two missed cleavages permitted, fixed carbamidomethylation on cysteine, dynamic oxidation of methionine, dynamic acetylation on the protein N terminus, and dynamic biotinylation of lysine residues. A false discovery rate of <1% was obtained for the uniquely labeled peptides and proteins. The LFQ intensity values were log-transformed for further analysis, and missing values were filled with imputed values representing a normal distribution around the detection limit. Protein intensity was determined using Perseus software.

RNF5 plasmid transfection and virus infection

A549-hACE2 cells were grown in Minimal Essential Medium (MEM) (ThermoFisher, cat. No., 21090022) supplemented with L-glutamine (2) (Cytiva, cat. No., SH30034.01), HEPES (10mM) (Scientific, cat. No., 15630056), 100U/ml penicillin and 100 g/mL streptomycin. Transfection of either functional RNF5 or nonfunctional RNF5 (containing the C42S mutation) plasmid constructs (tagged with mCherry or HA) was performed in A549-hACE2 using Lipofectamine LTX with PLUS reagents according to the manufacturer's protocols. Cells were grown in 24-well plates on coverslips in a regular growth medium until they reached 60–80% confluence. The cells were then transfected with 3 g of each plasmid (mCherry-RNF5, HA-RNF5, mCherry-RNF5(C42S)

and HA-RNF5(C42S)) using transfection reagents in the transfection medium without antibiotics. The medium was replaced with fresh medium at 5-to-5.5-h post-transfection. The cells were then infected with wild-type SARS-CoV-2 (isolate SARS-CoV-2/human/SWE/01/2020; GenBank accession: MT093571.1) at an MOI of 1 in complete growth medium. After 1 h incubation at 37°C, the medium was exchanged to fresh growth medium. Samples were collected 18 h after infection. All studies related to SARS-CoV-2 live virus infection were performed inside the biosafety level 3 facility of the Karolinska Institute, Stockholm, Sweden.

Immunofluorescence microscopy

The cells were washed with PBS and fixed with 4% paraformaldehyde for 15 min at room temperature. The cells were then permeabilized with 0.1% (v/v) Triton X- in PBS for 15 min and washed thrice with PBS. Blocking was performed by treating cells with 0.5% (v/v) fetal bovine serum in PBS for 30 min. The samples were then incubated with the primary antibodies diluted in 0.5% (v/v) fetal bovine serum in PBS: rabbit anti-SARS-CoV-2 nucleoprotein (kindly provided by Dr. Pamela Österlund, National Institute for Health and Welfare, Helsinki, Finland)[73] (1:200) and mouse anti-HA tag monoclonal antibody (Invitrogen, cat. No., 26183) (1:200). After 1 h of incubation with the primary antibodies at room temperature, the samples were washed to remove excess antibodies. The samples were then incubated for 1 h with DAPI and the following secondary antibodies at room temperature: goat anti-mouse Alexa Fluor 546 (Invitrogen, cat. No., A11030) (1:1000) and goat anti-rabbit Alexa Fluor 488 (Invitrogen, cat. No., A11034) (1:500). Imaging was performed using an Olympus AX70 Provis motorized widefield fluorescence microscope, and image processing was performed using Olympus cellSens Entry 1.18 software. The images were then analyzed using ImageJ software. Specifically, manual quantification of cells was performed by counting 10–20 microscope frames from each biological replicate, with a total nucleus number of more than 1000 in each replicate. Quantification analysis was performed for 4–5 independent biological replicates of each plasmid construct. The percentage of transfected cells harboring infections (positive for the SARS-CoV-2 nucleocapsid protein) out of all transfected cells was calculated.

Running AlphaFold2

AlphaFold v2.3.0 was downloaded from github and installed as a dockerized software under Linux (Ubuntu 22, AMD Ryzen 9 5950X, 128 GB RAM, NVidia RTX 4090 with 24GB RAM). Full databases were used using the flag "*db_preset = full_dbs*", and a total of 25 multimer models were generated using the flag "*num_multimer_predictions_per_model = 5*".

Data visualization

Protein visualization was done using UCSF ChimeraX(https://www.rbvi.ucsf.edu/chimerax). PAE values were visualized using the Python library alpha_viewer (https://github.com/Intron7/alpha_viewer, https://zenodo.org/record/7554913]).

Construction of web-based search platform of ORF3a and M interactome

(http://sarscov2.spatiomics.org)

The sarscov2.spatiomics.org web application is based on the JavaScript frameworks React (https://react.dev/) and ExpressJS (https://expressjs.com/). The experimental data are stored and accessed using a mySQL (https://www.mysql.com/) relational database. The iCn3D viewer was embedded using the npm package (https://www.npmjs.com/package/icn3d) to visualize the labeled sites on the AlphaFold structure. D3.js (https://d3js.org/) was used for heatmap visualization of MS data. PubMed queries are performed using the Entrez Programming Utilities API (https://www.ncbi.nlm.nih.gov/books/NBK25500/).

Transmembrane domain sources

Uniprot transmembrane domain annotation were downloaded from the website using the UniProtID mapping service(https://www.uniprot.org/id-mapping). TMbed transmembrane domain annotation were downloaded from the pre-calculated human proteome data (https://rostlab.org/public/tmbed/predictions/human_210422_tmbed.tar.gz). DeepTMHMM transmembrane domain annotation were calculated by running the biolib application (https://dtu.biolib.com/DeepTMHMM/) on a local machine (Ubuntu 22, AMD Ryzen 9 5950X, 128 GB RAM, NVidia RTX 4090 with 24GB RAM) as per given instruction on the website, using the UniProt primary protein sequence as input.

QUANTIFICATION AND STATISTICAL ANALYSIS

Significance was calculated by Student's t-test using GraphPad Prism 9 (GraphPad Software, USA). $p < 0.05$ were considered significant.